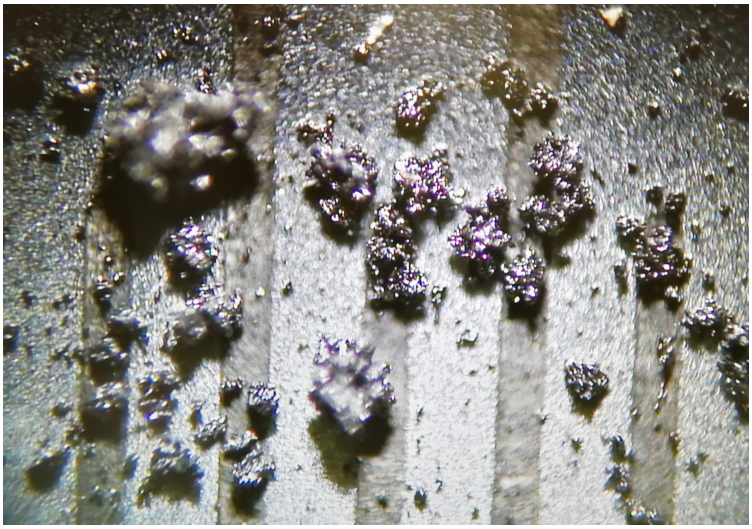

SEEX15-22-03 Experimental study for the production of calcium manganate particles and their use in chemical-looping combustion

Bachelor Thesis within chemical engineering, chemical engineering with physics, and mechanical engineering

Abubakar Abukar

Moa Andersson

Samuel Humpage

Andreas Jonsson

Eric Moilanen

Milly Lieback

Department of Space, Earth and Environment

Chalmers University of Technology

Gothenburg, Sweden 2022

www.chalmers.se

Supervisor: Daofeng Mei, *Division of Energy Technology*
Assistant Supervisor: Anders Lyngfelt, *Division of Energy Technology*
Examiner: Tobias Mattisson, *Division of Energy Technology*

Bachelor Thesis 2022: SEEX15-22-03
Department of Space, Earth and Environment
Division of Energy Technology
Chalmers University of Technology
SE-412 96 Gothenburg
Telephone +46 31 772 1000

Coverphoto: Light microscope picture of manufactured oxygen carrier particles.

Font in LaTeX
Gothenburg, Sweden 2022

Abstract

With higher demands for energy comes higher demands on current combustion processes, more specifically the demand to reduce the emission of CO_2. One solution is the chemical-looping combustion process (CLC) using oxygen carriers to isolate CO_2 in pure form. Thereafter carbon capture and storage (CCS) is applied, where the CO_2 is captured and stored deep in the ground or under the bottom of the sea. In this report the focus was to find a method to produce the oxygen carrier calcium manganate, $CaMnO_{3-\delta}$, in a way that results in cheap and strong oxygen carriers with chemical looping with oxygen uncoupling (CLOU) properties. To be able to implement $CaMnO_{3-\delta}$ as a competitive oxygen carrier it should be produced by manganese ore, since it could get to expensive with pure manganese. To find the best production method and the properties of the oxygen carriers, they were subjected to a series of laboratory tests. A method was chosen and multiple samples were produced using different combinations of temperature and manganese ore. The samples' physical attributes were tested and ranked. The three best samples were chosen and tested in a fluidized bed batch reactor to see how they could potentially react in a CLC system. In the reactor the oxygen carriers exhibited CLOU properties as was seen from the release of of oxygen to the gas phase. The samples showed an ability to release $\sim$ 2 wt% oxygen while approximately 10 % of that oxygen was release through oxygen uncoupling. The attrition test showed that the most reactive particles all had the highest degree of attrition, particles produced from Eramet ore sintered at 1265 °C, was shown to have an attrition rate of $1.35\frac{wt\%}{h}$ from a jet cup attrition test . An X-ray diffractometer verified that calcium manganate particles were present in all three samples. A techno-economic analysis of the production of oxygen carrier estimated a required concurrent mass in a 1 MW CLC system of 41 kg for the sample with the lowest cost. For the same sample a CLC system would additionally require a flow 8786 kg/year of fresh oxygen carriers due to the measured attrition rate. These results corresponds to a yearly cost of 1015066 SEK/year for the required materials and the production of the best sample in large scale. The main expense of was the cost of heating, calcining the limestone as well as sintering, as the yearly cost of the ovens is responsible for 87 % of the yearly cost. As discussed in this report, the best way to improve the results of the particles and lower the cost would be to research the lifetime by testing it in a real CLC environment and also continuing to further improve it. A suggestion for a way to approach this is to research the sintering process as this is tightly connected to lifetime.

Sammanfattning

Med ökad efterfrågan på energi ställer det även högre krav på dagens förbränningsanläggningar, mer specifikt högre krav på att minska utsläppet av CO_2. En lösning är kemcyklisk förbränning (CLC) som använder syrebärare i en process för att isolera CO_2. Därefter kan koldioxidinfångning och lagring (CCS) användas som fångar in CO_2 för vidare lagring under marken eller i havsbottnen. I denna rapport ligger fokus på att hitta en metod för att producera partiklar av syrebäraren kalciummanganat, $CaMnO_{3-\delta}$, på ett sätt som ger billiga och starka syrebärare med kemcyklisk syrefrånkoppling (CLOU) egenskaper. För att kunna implementera $CaMnO_{3-\delta}$ som en konkurrenskraftig syrebärare bör de produceras av manganmalm eftersom ren mangan annars kan göra den för dyr. För att hitta den bästa produktionsmetoden samt undersöka syrebärarnas egenskaper, genomgick syrebärarna diverse laborativa tester. En metod användes för att producera flera prov med varierande kombinationer av temperaturer och malmsorter. Provens fysiska egenskaper testades och de tre bästa proverna valdes ut, dessa testades sedan i en fluidiserad satsreaktor för att se hur de potentiellt hade reagerat i ett CLC-system, i reaktorn uppvisade syrebärarna även CLOU egenskaper. Proven visade en förmåga att frigöra $\tilde{2}$ wt% syre medan ungefär 10 % av syret släpps ut genom CLOU. Ett av de laborativa testen som gjordes var ett förslipningstest och det bästa provet, gjort av Eramet malm och sintrerat i 1265 C, visades ha en nerslipnings hastighet av $1.35\frac{wt\%}{h}$ när ett jet cup förslipningstest utfördes. En X-ray diffraktometer verifierade att det fanns kalciummanganat i de tre proven. Med hjälp av en teknoekonomisk analys av produktionen av syrebärare estimerade den ständiga massan som behövs i ett 1 MW CLC-system till 41 kg för det prov som visade lägst kostnad. Analysen av provet visade även att ett ytterligare flöde på 8786 kg/år av nya syrebärare partiklar krävdes på grund av ständig nerslippning. Dessa resultat motsvarar en årlig kostnad för produktion samt material på 1015066 SEK/år. Huvudutgiften består av värmekostnader då 87 % av de totala årliga utgifterna är kostnaderna för uppvärmingen av ugnen . Som diskuteras i denna rapport är det bästa sättet att minska kostnader vidare forskning på livstiden av partiklarna genom att testa den i en äkta CLC miljö och att också försöka förbättra den ytterligare. Ett förslag på ett sätt att angripa detta är att undersöka sintrerings processen som är starkt kopplad till livstiden.

Acknowledgements

We would like to extend thanks to Daofeng Mei and Anders Lyngfelt from the division of Energy Technology for helping and supporting us along the way, and providing us with the basis for this project. Also thanks to Tobias Mattisson for being the examiner and contributing with ideas that improved the project at large. We would also want to thank everyone in the M3 lab and in the chemistry lab, that have been very nice and helpful.

Contents

1 Introduction

The increasing amount of carbon dioxide in the environment is causing ocean acidification [1] as well as global warming [2]. This affects humans [3], animals and other living things alike [4]. This is common knowledge for most, however how to solve this problem is not. One step on the way is a technology called carbon capture and storage (CCS), as it eliminates the CO_2 from being released to the atmosphere from energy conversion processes. Chemical-looping combustion (CLC) which is one of the CCS technologies. This report and the experimental work behind it will attempt to provide a solution to a part of the problem, by providing a way to minimize the release of CO_2 into the atmosphere.

In a normal combustion process air is directly injected into the combustion chamber. Due to the large amount of inert nitrogen in the air, the desired combustion products, CO_2, H_2O, are diluted by mainly N_2, SO_x and NO_x gases from the air injected, therefore the product is hard to utilize or store. Chemical-looping-combustion is a technology which can result in inherent separation of the CO_2 from the flue gases. Oxygen carriers are particles that can absorb and release oxygen for combustion, meaning they can transport oxygen from the air to a combustion chamber, solving the problem of dilution [5]. In CLC, since the oxygen carriers transport only oxygen into the combustion chamber, there will only be carbon dioxide and water vapor exiting the combustion chamber. The water is removed by condensation, leaving a nearly pure stream of carbon dioxide that can be stored using CCS [6]. This way the carbon dioxide entering the atmosphere can be diminished and if biomass is used as fuel the combustion and storage process would lead to negative CO_2 emissions [6]. Due to this possibility of achieving negative emissions, there is a search for oxygen carriers that are economically viable for large scale CLC.

1.1 Background for CCS, CLC and oxygen carriers

CCS is the endgame for the CLC process. CCS is the process where the carbon dioxide is separated after the combustion in the fuel reactor and thereafter captured and stored in porous rock where it can remain for many generations (100-1000 years) [6] to come. CCS is needed to decrease the carbon dioxide-emission into the atmosphere and the ocean.

To obtain a better understanding of how oxygen carriers operate it is important

to have some insight into CLC. It is a system used for capturing carbon dioxide, since the process makes it possible to produce a concentrated stream of combustion products, free from nitrogen gas, which in traditional combustion would be a major fraction of the stream [5]. The CLC system consists of one air reactor and one fuel reactor, both of which are fluidized bed reactors [7]. The oxygen carrier particles in the bottom of the reactor chambers behave as a fluid when gas is injected from below. The oxygen carriers in the air reactor absorb oxygen after which they travel from the air reactor to the fuel reactor where the absorbed oxygen is released and reacts with the fuel, combusting it. The oxygen carrier particles then return to the air reactor and the process repeats [7]. A simplified model of this can be seen in figure 1 below.

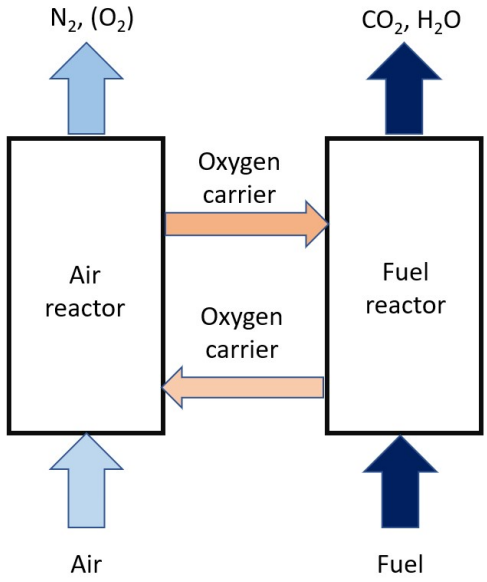

Figure 1: Chemical looping combustion process

Solid fuels can also be used for CLC. Fuel can either be converted in the fuel reactor together with oxygen carriers, or it can be gasified before it enters the CLC [8] Gasification is beneficial since it generates syngas and other gaseuous components such as methane, which react much more effectively with the oxygen carrier than the solid fuel. Gasification is performed by injection of a stream of hot CO_2 and water into a fluidized bed of the solid fuel and oxygen carrier particles. The generated gases then

react with the oxygen carrier as it forms. The gaseous product stream from the fuel reactor, consisting largely of CO_2 and water, then leaves the reactor and is cooled to condense the water, leaving the gas phase as mostly pure CO_2 [9].

Common reactors use air for combustion which is not desirable due to a mix of nitrogen, carbon dioxide and other compounds in the outflow of the reactor. Separation of gases is generally difficult and energy intensive, therefore not economically beneficial [9]. This is why oxygen carriers are of interest, with oxygen carriers it is possible to use air by separating the oxygen out of the air continuously transfer the oxygen through the oxygen carrier into the fuel reactor for pure oxygen-fuel combustion without need for expensive oxygen purification membrane equipment or even more costly electrolysis.

Oxygen carriers usually consists of a transition metal oxide or metal oxide mixture. [10]. Certain oxygen carriers have properties that allow it to absorb and release oxygen gas, which is desirable for CLC. The ability for a oxygen carrier to absorb and release gaseous oxygen within the CLC process is called Chemical Looping with Oxygen Uncoupling (CLOU) [9]. CLOU properties are desirable since it means that the oxygen release from the oxygen carrier is spontaneous [11], which it is not for oxygen carriers without CLOU properties. Oxygen uncoupling increases the efficiency and conversion of the reactor [12]. When the oxygen carrier does not have oxygen uncoupling properties, the only method of reaction is at the solid-gas interface. With oxygen uncoupling, the combustion takes place in the entire gas volume as well as the surface, making it more efficient than combustion only happening at the surface of the oxygen carrier. Oxygen uncoupling properties are also beneficial since they allow the release of oxygen from inside the particle through pores out into the gas volume, as otherwise the oxygen inside the particle would only react with the fuel that slowly enters the particel through pore-diffusion. This CLOU characteristic has been observed in calcium manganate but has been more thoroughly studied in copper oxide[9].

The spontaneous absorption and release of oxygen for the CLOU process occurs due to an equilibrium with the surrounding environment. For the oxygen carrier Calcium manganate the equilibrium is equation (1) below. When there is a high concentration of oxygen, such as in the air reactor, the equilibrium is shifted towards formation of a higher oxide, left in the equilibrium example below. In a low oxygen concentration environment, such as in the fuel reactor, the equilibrium is instead shifted toward release of oxygen and formation of a lower oxide, right in the below

example. The equilibrium is also temperature dependent, as the endothermic decomposition of the material is more favorable at higher temperature, thus shifting the equilibrium toward oxygen release [13].

$$CaMnO_3 \Leftrightarrow CaMnO_2 + \frac{1}{2}O_2 \tag{1}$$

A good oxygen carrier should possess the following traits. One, it should have a high reaction rate toward the fuel in use. Two, it should not be toxic for humans or the environment. Three, it should have a low manufacturing price, meaning it should cost less to produce than oxygen carriers produced from more noble metals like copper and nickel. Four, it should be easily fluidized in the two reactors. To be easily fluidized the particles can not be too big, in general not bigger than 300 µm [14]. Five, it should not be too small or it will escape with the exhaust gases from the CLC, particles smaller than 90 µm likely would not be suitable [14]. Six, it should not easily break down mechanically from collisions and attrition. If any of these traits are not met, the oxygen carrier will most likely not be used to a large extent [15].

1.2 Previous experimental results

Initial experiments, reviewed by for example Lyngfelt[9] [16], were mainly done with monometallic oxides such as NiO, CuO and Fe_2O_3. Both NiO and CuO have shown great results when it comes to reactivity but have the disadvantage of being relatively expensive while NiO is quite toxic [9]. Some combined oxides have been tested and have shown good results, many of which are based on manganese as the metal oxide. Manganese has shown better results than Fe oxides while being cheaper and safer than Ni and Cu [9]. Manganese oxide (MnO_2) by itself does not exhibit CLOU properties, however, the combinations of manganese with other transition oxides, such as calcium, does show oxygen uncoupling ability [9]. Along with having CLOU properties, another advantage of calcium manganate is that it is relatively easy to prepare from available manganese ores.

Experiments using $CaMnO_{3-\delta}$ have shown good results for reactivity and conversion but were primarily done by doping calcium manganate with either magnesium, titanium or both [17]. The results also showed lackluster performance with respect to attrition. An estimate of the particle lifetime of $CaMnO_{3-\delta}$ done by Hallberg et al [18], was around 1000 hours, meaning it would have to be completely replaced

several times during a year of operation. Experiments have also shown that the size of the particles are related to the hydrodynamics of the fluidization. The correct size can result in better particle distribution along the bed height leading to better combustion performance [19].

In previous experiments with calcium manganate, a spray-drying method has been used to produce spherical particles. This method involved producing a slurry of the reagents which was sprayed through a small nozzle forming fine drops of the slurry [20]. The drops dry into spheres which are then sifted to collect the desired particle size. Finally, the selected particles were sintered and the binder burned off, leaving hard and porous particles of the calcium manganate material. As the spray drying is a large scale method, it is not suitable for the optimization of a cheap manufacturing method for oxygen carriers [21]. Still, the use of spray-drying could be relevant for large scale processes, as it is commercial and readily available globally.

1.3 Purpose

The purpose of this project is to investigate an alternative method for producing $CaMnO_{3-\delta}$ as an oxygen carrier for a CLC system that is compatible with CCS. In finding the middle ground between the wanted oxygen carrying properties and potential cost of the oxygen carrier, cheap and promising materials will be explored so that CLC technology can become a more viable and attractive proposition for commercial use in the future. The optimal method to do this will be found through trial and error; by having a starting point and subsequently changing a few parameters at a time, such as temperature. While doing this, different test results will be collected and analyzed which will then be used to determine the optimal method. Ensuing finding this method, the physical attributes and the reactivity of the materials will be tested. The materials will vary as a few selected ores will be used in the production of oxygen carriers. The ores will be chosen based on their composition and availability. In total, this will result in a procedure for making calcium manganate as oxygen carriers from the studied materials as well as data of the materials physical and chemical properties which will be used for a techno-economic analysis. The purpose of a techno-economic analysis is to explore the possibilities to scale up the production to an industrial level.

The project will attempt to answer the following three questions and the method will also be divided into three stages according to these.

1. What is the best process for producing $CaMnO_{3-\delta}$ from inexpensive manganese and calcium ores instead of the relatively more expensive pure chemicals?

2. What are the physical attributes of the produced oxygen carrier particles; attrition rate, material strength and density of the particles? How well can these particles transport oxygen?

3. If they have suitable attributes, can the manufacturing process be scaled to make multi-ton batches, and what would that cost?

Constraints: This project is limited to the study of the production of $CaMnO_{3-\delta}$ particles and will therefore not include how and where to obtain the raw materials. The underlying reason for this limitation is the nature of the research; while this study is scientific, procuring the raw materials is an economic matter. For the purpose of focusing on the scientific nature, the process covered in this study will begin after procuring the needed raw materials. Production of the oxygen carriers will be done with one specific limestone ore and three different manganese ores, which are Buritirama, Eramet HM and Sibelco Braunite. These specific manganese ores are of interest due to their high manganese concentration, accessibility in the lab, availability for further research and use in the future. While all samples will undergo the physical tests, only a few samples will be tested to see oxygen carrying ability as this test is time consuming. The techno-economic analysis is also limited to the preparation process and will not cover the costs of building and maintaining a CLC facility.

2 Method - How the research of $CaMnO_{3-\delta}$ was done

This section describes a systematic method of the research of the production of oxygen carrier $CaMnO_{3-\delta}$ to answer each question stated in the purpose section of this project. As the type of method suitable to answer each question is different, this section is divided into three stages.

In the **first stage** a method was used to find a suitable manufacturing process to make the oxygen carrier, calcium manganate. New ways to manufacture calcium manganate was researched by performing experiments with different parameters. Each experimental manufacturing process was then evaluated by using tests such as attrition, crushing strength and particle size distribution to determine how suitable each of the processes could be. Finally, these resulted in the most suitable manu-

facturing process which will be presented in the results. Different parameters were changed to find the optimal manufacturing process, these include PVA solution and granulation procedure.

Moving on to the **second stage** the focus was shifted from researching the most suitable manufacturing process to researching what oxygen carrier made with the process was most suitable for CLC. Three ores were sintered at different temperatures, resulting in nine samples of oxygen carriers. These ores were Sibelco Braunite, Buritirama and Eramet HM. The oxygen carrier samples were tested using attrition, crushing strength test, density test, batch reactor test, X-ray diffraction (XRD) analysis and Scanning Electron Microscope (SEM) for composition and structure analysis.

Lastly the **third stage** describes how a techno-economic analysis was done to estimate the cost for scaling up the production to an industrial scale. This analysis was done on the basis of producing enough $CaMnO_{3-\delta}$ for a 1 MW CLC system.

2.1 Stage 1 - How the manufacturing process was researched

By reading previous research done by Moldenhauer et al [17] and KEMIRA chemicals [22] the general manufacturing process for the oxygen carrier was decided. KEMIRA chemicals [22] provided a starting point for how to granulate the powder mixture. The general manufacturing process, including the KEMIRA method can be seen in figure 2 below.

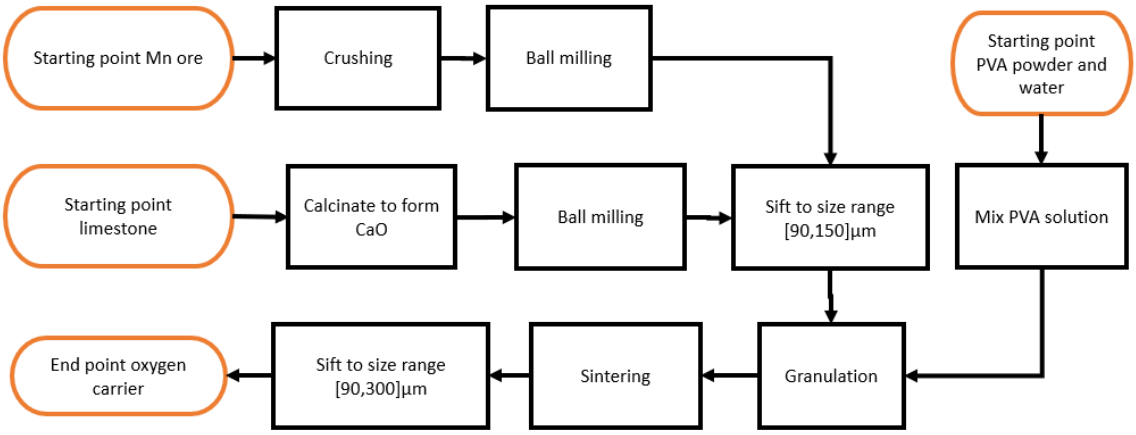

Figure 2: The manufacturing process visualized with a flow chart

Starting with raw materials, such as different manganese ores, limestone and PVA, the raw materials had to be prepared for granulation. The manganese ore was crushed into smaller pieces and limestone was calcined to get calcium oxide. Both manganese ore and calcium oxide were then ball milled and sifted to get the preferred sizes. Smaller sizes are desirable since there is an increased contact area per volume and therefore the reactivity between the calcium and the manganese ore is higher. PVA powder was mixed with water and was subjected to heat until dissolved. This PVA solution will work as the binder for the sifted ores and calcium oxide in the granulation.

After the preparation of the materials, the granulation could begin. The granulation process is the mixing and forming needed for the ingredients to combine into particles, soon to be oxygen carriers. The granulated particles were then sintered to react into new possible oxygen carriers. Lastly the oxygen carriers where sifted to collect the size range of [90,300] μm.

Different oxygen carriers were made by changing parameters for the general manufacturing process. The main parameters changed to test this manufacturing process were amount [wt%] of PVA solution and the type of granulation procedures used. Four different amounts of binder solution and two procedures were tested. Only one manganese ore and one sintering temperature was used when combinations of PVA solution and granulation were tested.

Testing the physical attributes of the oxygen carriers, made by changing parameters, provided a basis to determine which manufacturing process was the most suitable. The oxygen carriers were examined by testing the crushing strength and the attrition rate. The crushing strength is important since it correlates to how well it can withstand mechanical breakdown. The attrition is important for examining how much the oxygen carrier degrades in airflow conditions close to a fluidized bed reactor. After sifting and weighing the oxygen carrier, the $wt\%$ was calculated for each size range and was also taken into consideration when choosing the best manufacturing process. The size range is important partly because of the size constraints for fluidization, meaning it should not be too small, or it will follow the outflow from the CLC. They should also not be too large as this would inhibit fluidization.

The most suitable manufacturing process should be one yielding an oxygen carrier with high crushing strength, low attrition rate and as much particles within the size range as possible. The amount of PVA binder used was also taken into consideration.

The best manufacturing process within the criteria limits was thereby chosen, the details are presented in the results.

2.1.1 The manufacturing process in detail

To get a better understanding of each step in the manufacturing process a more thorough explanation is described in the coming paragraphs.

Calcination of limestone ore was one of the first steps performed in the manufacturing process. In previous research, $CaMnO_{3-\delta}$ has been synthesized using calcined limestone [23]. The calcium in limestone has extra carbon and oxygen bound to it, that releases during the calcination process leaving CaO. The limestone was calcined in a steel crucible at 800°C for 2 hours then 950°C for 9 hours using a programmable high temperature oven. This was done to prevent release of CO_2 during sintering. The reason for the prevention was a speculation that the gas release could impact the oxygen carriers physical properties. To test this speculation, one iteration of the manufacturing process was done using uncalcined limestone.

Ball milling was a key part in the size reduction of the manganese ore, and the calcium oxide after the calcination. Ball milling was done in a ceramic jar half filled with the material and ceramic balls. The jar was then rotated on rollers so that the ceramic balls crushed the material inside of the jar. This crushed the material into a smaller size, as was desired for the manufacturing process. To speed things up, some of the manganese ores were reduced in size from bigger ores chunks to smaller pieces by using a plate crusher before use of the ballmill. Moreover, depending on the hardness of the ores, the ball mill had to run for differing lengths of time. Approximately around 24h per filled jar for all the ores, some longer depending on how fine the particles looked when visually inspected. The time also depended on when the ball mill was started, since the time of the project was limited and the ball mill was running overnight or even over a weekend if needed.

Sifting was used on the particles after ball milling and on the oxygen carrier after sintering. Sifting was done so that particles smaller or bigger than the chosen range could be separated and removed. Sifting uses trays with a metal screen in the bottom that let particles smaller than the grid size of the screen through the tray. The acceptable size range for oxygen carriers was [90,300]µm. The manganese ores and calcium oxide had a different size range, [90,150]µm, this range was chosen partly

to not make oxygen carriers smaller or bigger than the desired oxygen carrier size range. To do the separation, the trays were stacked from bottom to top; smaller to larger grid size and the particles were then added. To make the particles able to pass through the screens, motion was introduced by a machine that vibrated the stacked trays for 15 minutes.

Granulation was performed after sifting. Granulation is a procedure used for mixing and adding ingredients with the intent of creating granules. The ingredients used where the sifted ore, calcium oxide and a binder solution with 10 wt% PVA. Note that the 10 wt% here refers to the amount of PVA in the solution, not the amount solution in the mix. The ore and calcium oxide were the building blocks for the granule and the PVA solution was the glue that held these together. Two types of procedures were used; batch added material (BaM) and continuously added material (CaM). The BaM and CaM procedures have a lot of similarities as well as a few differences. A notable similarity was that both these methods used the same stoichiometric ratio of manganese (in the ore) and calcium oxide.

- For the **BaM** procedure all the components were added in one batch while mixing. The dry ingredients were added into the food processor and whisked until evenly distributed. The PVA solution was added to the mix while whisking. By spraying the PVA solution with a spray bottle into the mixture, the PVA was distributed evenly through small droplets. After further mixing, the granulation was complete.

- For the **CaM** procedure the components were added continuously while mixing. The idea of this procedure was that the granules could be built in layers, by alternating adding dry ingredients and PVA solution. All the dry ingredients were added into a plastic container and mixed with a fork until evenly distributed. Around 1/4 of the mixed dry ingredients was transferred into a new container and sprayed with PVA solution. After mixing, new dry ingredients were then alternately added in small amounts together with sprayed PVA solution while continuously mixed with a fork. This was repeated until all the ingredients was used up. After further mixing the granulation was complete.

Similarly, four different PVA solution amounts were tested. Using the BaM method PVA was added in batches. When the mixture had become homogenous, the added amount was noted, and a sample extracted before adding even more. This was repeated four times resulting in four wt% of PVA samples.

Sintering was conducted after granulation. The process of sintering combines ingredients by heating them up making it possible to fuse into $CaMnO_{3-\delta}$. The temperature should not be too high since it causes the particles to melt. A sintering temperature of 1215 °C was used in stage 1 of the method. The oven was programmed to ramp the temperature up to 800 °C and dwell there for 2h then ramp up to the decided sintering temperature, were the sample dwelled for an additional 9h. Lastly the temperature was ramped down to room temperature.

2.1.2 Determining the suitability of the manufacturing process

In this section the two procedures BaM and CaM are compared. To compare them, three different tests were performed: attrition test, crushing strength test and size distribution. These are described in detail below.

Attrition tests were done by simulating a fluidized bed reactor and observing how much weight was lost due to attrition. To perform the attrition test, roughly 5g of sintered particles in the sizes of [90,300] µm are measured. These particles were then placed in a jet cup and fastened to the rig, shown in figure 3 below. Testing the attrition rate of the particles was done during one hour, where the particles were subjected to an airflow of 10 liters per minute which would cause the particles to break down through collisions between themselves and with the walls of the apparatus. These collisions produced fines that were transported with the air through an air filter which was weighed every 10 minutes after start. To determine the stable attrition rate the mass gain in the filter between the last two measurements, namely 50 and 60 minutes, was divided by the remaining mass of particles inside the apparatus at that time and the duration that gain took (1/6h). The attrition rate was calculated at the end of the run due to the rate being far higher toward the beginning as small dust like particles are being easily blown away, while the useful larger particles remain inside the apparatus throughout the full run. To calculate the attrition rate for a sample, equation (2) below was used to calculate the mass of the remaining particles after 50 min. Equation (3) was then used to calculate the final stable attrition rate.

$$m_{particles,50min} = m_{particles,0min} - (m_{filter,50min} - m_{filter,0min}) \tag{2}$$

$$\text{Attrition rate (\%/h)} = \frac{(m_{filter,60min} - m_{filter,50min}) * 100}{\frac{1}{6}h * m_{particles,50min}} \tag{3}$$

Crushing strength tests were performed to examine how well the oxygen carriers could handle mechanical stress. The crushing strength test was done by collecting a small amount of particles in the size range of [180,250]µm. A few particles were then placed on a small metal plate (the top of the apparatus), shown in figure 4 below and crushed with a blunt needle. The machine recorded the peak force that was used to break the particles while a digital Newton scale showed the results.

Figure 3: Picture of the customized jet rig which is used to perform the attrition test on the particles.

Figure 4: Picture of the crushing strength apparatus with the needle hanging to the right.

Size distribution tests were performed by sifting and weighting the sifted parts. This to examine how much wt% of the oxygen carrier sifted to the range [90,300]µm was in the size subrange [180,300]µm. This range was chosen to test how the granulation process affected the increase of particle size in the oxygen carrier after sintering. The lower bound of 180 µm was chosen to be higher than 150 µm, which is the upper size boundary for the dry ingredients. This was to not make an overlap of the ingredients size range and the subrange [180,300]µm being tested. An overlap could introduce a dependence between the ingredient size and measurement which was not the purpose of this test.

The decision matrix used the data from the described tests above and took into consideration the amount of PVA solution used to determine which procedure was the best. The decision matrix is a structured way of making the decision of what procedure to use. Each sample was evaluated based on four attributes. Each method

got a score based on equation (4).

$$\sum_{i=1}^{4} S_i W_i = R \tag{4}$$

Where i is the attribute, W is its weight and S is the score, finally R is the score of the method. W was a number between -1 and 1, chosen based on the importance of the attribute for the success of the procedure. The scoring of each sample was done using linear interpolation according to equation (5).

$$S = 1 + (x - min)\frac{10 - 1}{max - min} \tag{5}$$

Min was the lowest value and max was the highest test value of all processes in that attribute. Similarly, the variable x was the test value of the process being scored. This makes it so all methods get a score on each attribute. This score was between 1 and 10. An example of how such a decision matrix can be constructed is shown in table 1 below.

Table 1: Example of how three processes can be evaluated using a decision matrix. Process 3 has the highest result.

Attribute:	Attribute 1	Attribute 2	
Weights:	W1=-0.2	W2=0.5	
Process	Score		Result
Process 1	S1=10	S2=1	R=-1.5
Process 2	S1=1	S2=6	R=2.8
Process 3	S1=3	S2=10	R=4.4

The four attributes that were used when making the decision matrix were mean crushing strength, attrition rate, wt% in size sub range [180,250]µm and amount of PVA solution added.

The conclusion of this first stage was a decision of what manufacturing process was suitable to use for further testing on the oxygen carriers. The results from the decision matrix and a consideration from the boundaries of the project gave a final decision.

2.2 Stage 2 - Physical attributes and reactivity

After the oxygen carriers were produced using different ores and sintering temperatures, they were examined to determine the best of the produced samples. First the oxygen carriers went through attrition testing and a crushing strength test. Secondly, the particles were compared to each other to find the three best samples to use for further testing. Lastly, the three samples were subjected to a reactivity test to find the best oxygen carrier, and thereby the preferred manganese ore and temperature, and a bulk density test to use this data for further use.

2.2.1 How samples were produced, and how their physical properties were tested

Previously done tests were performed to find the best manufacturing process. The tests in this stage were done to evaluate the materials attributes. Ores and temperatures were the parameters that was changed between samples. So far, the temperature 1215 °C worked good, but a change in temperature has a big effect on oxygen carrier properties, therefore different temperatures had to be tested. These temperatures were determined by increasing or decreasing sintering temperature iteratively based on strength and degree of agglomeration. The manganese ores have different compositions; while they all have a high amount of manganese they have a different amount of other compounds, such as iron and silicon. All samples were tested with attrition and crushing strength tests. Only three of these samples could be chosen for the batch reactor due to the time constraints of this project. This was decided using the attrition values.

Bulk density testing was done on the manufactured samples of oxygen carriers. The bulk density of the particles was tested by weighing a container with a known volume filled with oxygen carrier particles. The container was filled and weighed 5 times per sample to get a mean value of the mass. This mean mass value together with the already known volume was then used to calculate the bulk density of each sample which can be seen in equation (6).

$$\rho_{bulk} = \frac{mass}{volume} \tag{6}$$

Batch reactor test was used to measure the chemical properties of the oxygen carriers and get an understanding of how the samples could perform in a CLC reactor. The chemical properties of the particles were analyzed by the use of a small quartz

tube fluidized-bed reactor, where air, nitrogen and fuel gas (methane and syngas) were intermittently injected. The composition and flow rate of the exiting gas was measured and logged for later analysis. The measured components were CO, CO_2, CH_4, O_2 and H_2. Due to the composition meter being at ambient temperature, the produced water vapor concentration was not logged as it had to be condensed from the flow before detection. The three reactive characteristics studied were the release of oxygen gas from the oxygen carrier (that is the CLOU properties), the reaction with methane gas and lastly the reaction with syngas. In order to determine if the material could be suitable for CLC, the CLOU properties were studied both before and after reaction with the fuel gases. The reaction with syngas was studied for both unused oxygen carrier as well as the used material from methane reaction. This as done because the reaction with methane has previously showed to change the reactive and CLOU properties of other CLC materials [24].

Before starting any reaction, the flow meter and gas detectors were calibrated and the reactor was tested for potential leaks by injecting a calibrated flow rate of nitrogen gas and checking that the measured flow rate matches. The samples to be reacted with methane gas were prepared by loading 20g of particles into the reactor, while the samples to be reacted with syngas had to be diluted with 5g oxygen carrier to 15g silica sand. This because the higher reactivity of syngas may otherwise have combusted the fuel completely, which induces difficulty in the data analysis. The general procedure for measuring the oxygen absorption and release was to first heat the reactor to 950°C with nitrogen flow. After reaching the target temperature 10.9% oxygen and 89.1% nitrogen was injected for approximately 300 s in order to charge the oxygen carrier to their equilibrium oxygen content. To measure the release of the absorbed oxygen pure nitrogen was subsequently injected for 800 s or until the output oxygen concentration was below 0.1%. This cycle was repeated 3-4 times before and after the methane reaction and 2 times[1] after the syngas reaction in order to get an average value.

The reaction with methane and syngas were both studied by the same gas injection program, first charging the particles with oxygen by injecting 300 s of 10.9% oxygen. Due to possible explosion risk, the oxygen remaining in the reactor was flushed out with 120 s of pure nitrogen gas, after which the fuel gas was injected for 20 s and system flushed again with 120 s of nitrogen gas. This program was repeated until the peak CO_2 values produced were stable, usually 3-4 cycles.

[1]Except for in the case of the S9-fresh sample, where the CLOU result was calculated during the oxygen uncoupling phase before the third reaction due to data collection issues.

2.2.2 Oxygen release

Using the volumetric flow data logged by the batch reactor as well as the concentration data measured by the gas analyzer, the total molar flow of oxygen gas exiting the reactor was calculated by the ideal gas law. To calculate the mass based oxygen uncoupling ability, the molar flow data during the oxygen release phase was integrated from the flow corresponding to 1 vol% O_2 to 0.1 vol%. To minimize errors due to oxygen residence time, the same integral calculated from a cold run was subtracted. Since the oxygen uncoupling only happens at elevated temperature, this cold run integral should correspond to the effect of residence time in the reactor. The total molar amount of oxygen gas released during the uncoupling phase is then multiplied by the molar mass and divided by the mass of oxygen carrier loaded in the reactor. This is shown in equation (7).

$$\text{Oxygen uncoupling ability (wt\%)} = \int_{t_0}^{t} \frac{\dot{n} M_{O_2}}{m_{ox}} x_{O2} dt * 100 \tag{7}$$

To calculate the oxygen carrier conversion ω as a function of time during the oxygen uncoupling phase equation (8) below was used.

$$\omega = 1 - \int_{t_0}^{t} \frac{\dot{n} M_O}{m_{ox}} x_{O2} dt \tag{8}$$

For the methane and syngas reaction, equations (9) and (10) were used respectively [25]. The molar flow of oxygen for all equations was corrected by subtracting the flow present during the cold run. It should be noted that this calculation is not perfect due to the requirement of assumption of how much water is produced in the reaction. If the amount of water formed had been measured, another equation should be used to determine the ω.

$$\omega = 1 - \int_{t_0}^{t} \frac{\dot{n} M_O}{m_{ox}} (4x_{CO2} + 3x_{CO} - x_{H_2}) dt \tag{9}$$

$$\omega = 1 - \int_{t_0}^{t} \frac{\dot{n} M_O}{m_{ox}} (2x_{CO2} + x_{CO} - x_{H_2}) dt \tag{10}$$

To determine the rate of oxygen release, the calculated omega value was differentiated

with respect to time using equation (11) presented below.

$$\dot{\omega} = \frac{d\omega}{dt} \tag{11}$$

To calculate the oxygen transport capacity, that is how much oxygen the material can hold and carry into combustion with fuel gas, equation (12) was used with the final ω obtained by equations (9) and (10).

$$\text{Oxygen transport capacity}^2 \ (\text{wt}\%) \ = (1 - \omega_{t,end}) * 100 \tag{12}$$

2.2.3 Fuel conversion

The quality of an oxygen carrier can be determined by how good it is at converting fuel to carbon dioxide, this is represented by the γ-value. The fuel conversion γ is defined by the mole fraction of carbon dioxide divided by the mole fraction of all carbon containing components in the flow. This can be seen in equation (13) for reaction with methane [26] and equation (14) for reaction with syngas [27].

$$\gamma_{CH_4} = \frac{x_{CO_2}}{x_{CO_2} + x_{CO} + x_{CH_4}} \tag{13}$$

$$\gamma_{syn} = \frac{x_{CO_2}}{x_{CO_2} + x_{CO}} \tag{14}$$

For the equations (13) and (14) the mole fraction for carbon dioxide has the abbreviation x_{CO_2}, the other carbon compounds (CO, CH_4) in the outflow are displayed in the same way. To analyse the combustion behavior of the oxygen carriers between the fully oxidized state ω=1 and the completely depleted state $\omega_{t,end}$, the fuel conversion γ was plotted against the ω value at that instance.

[2]Oxygen transport capacity based on the oxygen given off for reactions, not total oxygen content available. For the syngas reactions the values are close to the true transport capacity, but due to methane's lower reactivity the value obtained from those reactions will be significantly off from the true available oxygen.

2.2.4 How the chemical composition and particle structure was measured and analyzed

Each sample tested in the batch reactor was subjected to a chemical composition analysis using SEM and XRD. This was mainly done to see if $CaMnO_{3-\delta}$, the chemical intended to be researched, was present in the produced samples. The SEM and XRD data and analysis complimented each other. The analysis of the SEM data gave the atomic concentrations for the elements present in each sample. Further, the XRD analysis created possible matches between chemicals in a database containing the elements found in the SEM. SEM then performs an Energy Dispersive X-ray (EDX) analysis which results in a table of the elemental composition in the sample.

Zooming out from the molecular level to the particle level, images of the oxygen carrier particles were taken in the SEM. The purpose of these images was to see in what way the material had agglomerated during manufacturing into particles and what size they were. Also, the abundance of pores and cracks were studied for each sample. To do this, the three chosen samples were tested in both SEM and XRD before and after reaction with methane.

SEM was as mentioned the first one used. Each sample were embedded in epoxy and ground to expose the cross section of the particulates. Using a tabletop SEM many close up images of the cross section was studied. First a cross section image, 537 by 537 µm, was taken and then analyzed for composition. Then particles in the 537 by 537 µm area was analyzed by shrinking the image to the size of the particles and then taking another picture and composition analysis. This was done for many particles. Note that for all compositions analyzed the elements Am, B, Br, C, Hf, In, Pu, Rb were disabled.

XRD was done using an all-purpose X-ray analyzer, BRUKER D8 Discover with 1.54Å Cu radiation. The data provided by this XRD-test was analyzed in the software DIFFRAC.EVA. First a graph of the intensity against the diffraction angle was made, this allowed the software to match known graphs with a database containing graphs with crystals and powders of different elements. The database PDF-4+ 2022 was filtered to narrow down the possible matches. The filter was decided based on the elements present in the SEM composition analysis. Oxygen was marked mandatory and the elements from the SEM were marked neutral, meaning elements may match. All the other elements not found in the SEM were marked red, meaning they would not be detected in the XRD. The software calculated a figure of merit (FOM) for all the matches. The top matches based on FOM were then visually examined to

see what peaks of the sample graph they were matched to.

2.3 Stage 3 - Techno-economic analysis

The techno-economic analysis consists of two parts: The first step involves calculating the the amount of material that was required to produce enough $CaMnO_{3-\delta}$ particles in order to maintain a CLC reactor at a 1 MW output for 8000 hours per year. The second step then calculates the operating costs in order to produce said amount of oxygen carrier particles using suggested machinery.

2.3.1 Material cost

The cost of materials was evaluated by calculating the amount of oxygen carrier required to reach the necessary oxygen concentration in the fuel reactor. This was done by using the results of both the reactivity tests and attrition tests. How reactive the particles are towards the fuel determines the concurrent mass of oxygen carrier that needs to be in the reactor at any point in time; the more reactive the particles the less mass is needed. The amount of particles was calculated by evaluating how much of the fuel is required to produce 1 MW and thereby using the reaction formula, which can be seen in table 2, to calculate how many moles of oxygen is needed. From the reactivity test it was then possible to derive how much of the batch reactor tested oxygen carrier, $CaMnO_{3-\delta}$, was needed to release the calculated oxygen amount. This calculation assumed that the the calorific power input equal the power output.

Table 2: Reaction enthalpy occuring in fuel reactor

Reaction	H_i kJ/mole(O_2)
$CO + \frac{1}{2}O_2 \rightarrow CO_2$	-131.296
$H_2 + \frac{1}{2}O_2 \rightarrow H_2O$	-393.51

where H_i is the reaction enthalpy. The reactions which can be seen in table 2 results in each mole of oxygen releasing $521.806kJ$, assuming a 50/50 ratio of H_2 and CO in the syngas. The required oxygen flow in order to maintain a 1 MW output given the energy per mole oxygen was then calculated by equation (15) below.

$$\frac{1MW}{H_i \left[\frac{kJ}{molO_2}\right]} = F_{O_2} \left[\frac{molO_2}{s}\right] = \frac{F_{O_2} \left[\frac{g}{s}\right]}{M_{O_2} \left[\frac{g}{mol}\right]} \tag{15}$$

where F_{O_2} is the necessary flow of oxygen to support the combustion and M_{O_2} is the molar-mass of an oxygen molecule. From the calculated oxygen flow in equation (15) and the calculated oxygen transport capacity which is the weight percentage of oxygen per gram of oxygen carrier calculated from equation (12), the needed mass of oxygen carrier can then be calculated as follows in equation (16).

$$m_{CaMnO_{3-\delta}} = \omega \frac{F_{O_2} \left[\frac{g}{s}\right]}{\frac{d\omega}{dt} \left[\frac{wt\%}{s}\right]} \tag{16}$$

where ω represents the ratio of current mass to the mass of fully oxidized material, $\frac{d\omega}{dt} \left[\frac{wt\%}{s}\right]$ represents the release rate of oxygen from the oxygen carrier and $m_{CaMnO_{3-\delta}}$ the mass required of oxygen carriers. As only $\frac{d\omega}{dt}$ is analysed for the reduction process of the oxygen carriers in the reactivity tests, the rate of oxidation must be assumed to calculate the mass for the air reactor. The oxidation rate will be assumed to be equal in magnitude to the reduction rate since previous studies on calcium manganate materials have utilized reactors with similar fuel/air bed size[28].

Furthermore, when taking attrition rate into account, additional flow of oxygen carrier needs to be added continuously during the process, to make up for the constant decrease due to attrition. This flow is given by equation (17)

$$m_{CaMnO_{3-\delta}} [kg] \cdot \text{Attrition rate} \left[\frac{wt\%}{h}\right] = F_{CaMnO_{3-\delta},fresh} \left[\frac{kg}{h}\right] \tag{17}$$

As attrition rate is only measured in a jet cup attrition rig it will not give a fair representation of the potential lifetime in an actual chemical-looping process. However, since it was not possible to test the particles in a chemical-looping combustion process, the jet cup attrition value will be used for calculations. Other ingredients needed are directly dependent on the amount of oxygen carrier needed. For $CaMnO_{3-\delta}$, limestone is mixed with manganese in a stoichiometric ratio meaning it can be calculated using the molecular mass. The used PVA-volume depends on the volume of the mix of manganese and limestone and will be known after the Stage 1.

The cost of materials was then found by multiplying the needed materials with their respective price.

From the calculated concurrent mass required and the additional flow of oxygen carrier needed due to attrition the cost of material was then calculated. The cost of manganese ore is estimated at $4.5 per metric ton unit[29], Limestone at $34 per tonne [30] and PVA at $14 per 100 g [31]. The exchange rate used for these calculation is 9.82 SEK/$.

2.3.2 Manufacturing cost

The cost of manufacturing will not involve the initial cost of purchasing all machinery involved and instead focus on the cost of maintaining and operating them in order to produce the required amount of oxygen carriers calculated in the previous step. As this was a new proposed way to produce oxygen carriers, which in itself has limited previous research done, rough estimations were made during evaluation. Technology that was assumed during calculations were also merely suggestions that need further research. The cost of production was assumed to be dominated by the high temperature ovens used for both calcination and sintering, for this reason the calculations will mainly cover these expenditures. The cost of mixing, sieving and ball milling will still be analysed as it is vital for discussing the possibilities of up-scaling, but not as a main focus.

The proposed machinery for the calcination of limestone is a mesh belt furnace, in which the limestone is placed on a belt that travels through the oven. Using a mesh belt furnace with a capacity of 200 kg for calcination means the cost of electricity, maintenance and operation per hour will be $65.14 /h [32]. In a similar way the sintering is done in a pusher furnace, which works in a very similar way and cost $ 81.64/h with a capacity of 90 kg. With the cost and the capacity the yearly cost along with the initial cost can be calculated. The initial cost consist of the cost for buying enough material and producing the first batch which has the same mass as the concurrent mass.

For the rest of the machinery, namely mixer, sieve and ball mill, these costs are only done for their electricity cost. The electricity cost is done by researching different machinery to find the capacity and output and thereby calculating the residence time and cost. By evaluating the residence time from the capacity and required mass, the cost can be calculated by multiplying the output with the residence time and

the cost of electricity. The cost of electricity used for the ball mill, mixer and the sieve is 2.1 $\left[\frac{SEK}{kWh}\right]$ and is based on prices for Gothenburg in December 2021[33]. For the ball mill the considered machinery is an industrial ball mill with an output of $18.5kW$ and a capacity of 0.4 $\left[\frac{ton}{h}\right]$ [34]. Finally, machinery that could be used for the mixer is a horizontal mixer with an output of $45kW$ and a capacity of $8000L$ [35]. Lastly the proposed sieving machinery has an output of $4kW$ and an area of $2.3m^2$ [36]. For the sieve, the volume of the mass can be calculated from the density and subsequently the capacity of the sieve can be calculated by estimating a maximum height of $5cm$ for the cake that builds on the sieve. With the calculated capacity and outputs, the cost can be calculated in a similar way for the mixer, sieve and ball mill.

3 Results

In this section of the report the results from the method is presented. These results are the basis for the discussion section. The method gave a wide range of results such as test data, graphs, images, and decisions. These results have been summarized for ease of understanding and selected based on their importance for the discussion. The results will be presented in the same order as the enumerated questions in the purpose subsection of the introduction.

3.1 The manufacturing process results

The study of the manufacturing process, as described in the method section Stage 1, resulted in nine oxygen carrier samples ($P1, \ldots, P8, P13$) made from the manganese ore Buritirama. The manufacturing of these samples resulted in four PVA solution amounts and general observations. Testing the nine samples resulted in attrition, crushing strength and size distribution data. Finally resulting in a decision of the most suitable manufacturing process for this project.

The first results are the four selected amounts of PVA solution and how they visually affected the granulation. In figure 5 there are four granulated mixtures using BaM with the selected amounts. From left to right the corresponding amounts are 3.6, 8.1, 14.5 and 20.7 wt%.

Figure 5: Four different samples after granulation using BaM. The PVA solution content in wt% is displayed in the green text.

From this observation a higher amount of PVA solution results in a darker brown colour and a more coarse-grained texture. Light microscope examination of the 20.7 wt% mixture in figure 5, shows that the mixture mainly consist of visible manganese particles surrounded by and agglomerated with a finer brown compound, an example of this is shown in figure 6. This compound is presumed to be made of manganese ore fines, PVA and the calcium oxide. Manganese ore fines refer to the smaller powder stuck to the bigger particles in the Mn ore part of figure 6.

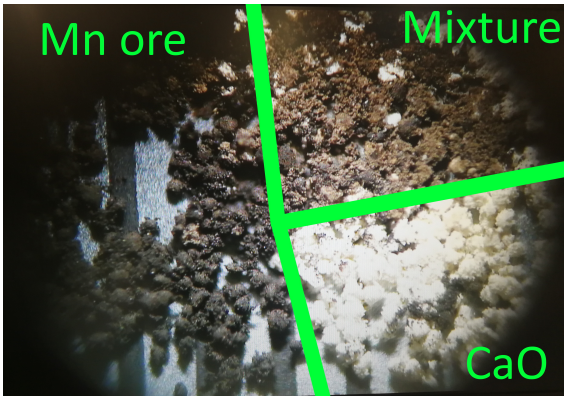

Figure 6: Manganese ore and calcium oxide sifted to the range [90,150] μm is shown to the left and lower right respectively. The mixture from using BaM method with 20.7 wt% PVA solution is shown is shown in the top right. Beneath is a scale with 0.5 mm graduations.

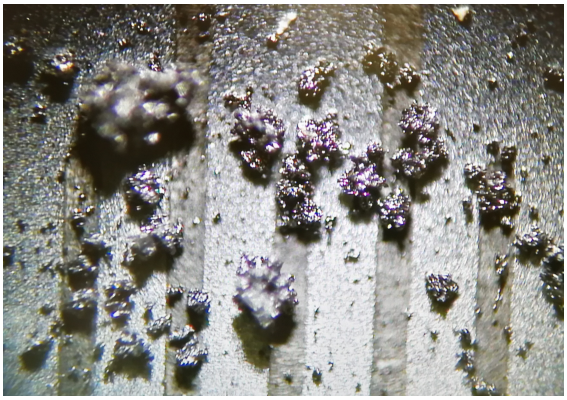

Figure 7: Oxygen carrier particles after sintering. Beneath is a scale with 0.5 mm graduations.

During granulation mixing, it was observed that the temperature of the mixture

increased as PVA-solution was added. After sintering the sample took on the appearance of gray cake, as can be seen in 8 below. The cake, as it will be referred to, is brittle but cohesive after sintering at a temperature of 1215 °C. Light microscope examination of the oxygen carrier particles extracted from the cakes shows round particles with a rough and granular surface. They are of different sizes and have a grey colour and a metallic luster. These particles can be seen in figure 7 above.

Figure 8: Three samples after sintering. The samples are made from different manganese ores and where sintered at different temperatures. Samples left to right: S5 is eramet ore at 1215 °C, S6 is braunite ore at 1215 °C, S7 is buritirama ore at 1265 °C

Moving on, the nine samples are the possible combinations of the two granulation procedures and four PVA solution amounts with the addition of sample $P13$. This sample resulted from skipping the calcination step in the manufacturing process in figure 2 and used the CaM procedure with 8.1 wt% PVA solution. Each of these samples have the results from their attrition rate and crushing strength tests shown in table 4. Additionally, $P1, \ldots, P8$ have results from the size distribution test. This is plotted as wt% particles against wt% PVA solution in figure 9. The BaM procedure gives a higher wt% particles in the subrange [180,300]µm than CaM. Both procedures result in a concave graph. From 3.6 to 8.1 wt% solution there is an increases in wt% particles, while from 14.5 to 20.7 wt% solution there is a decrease.

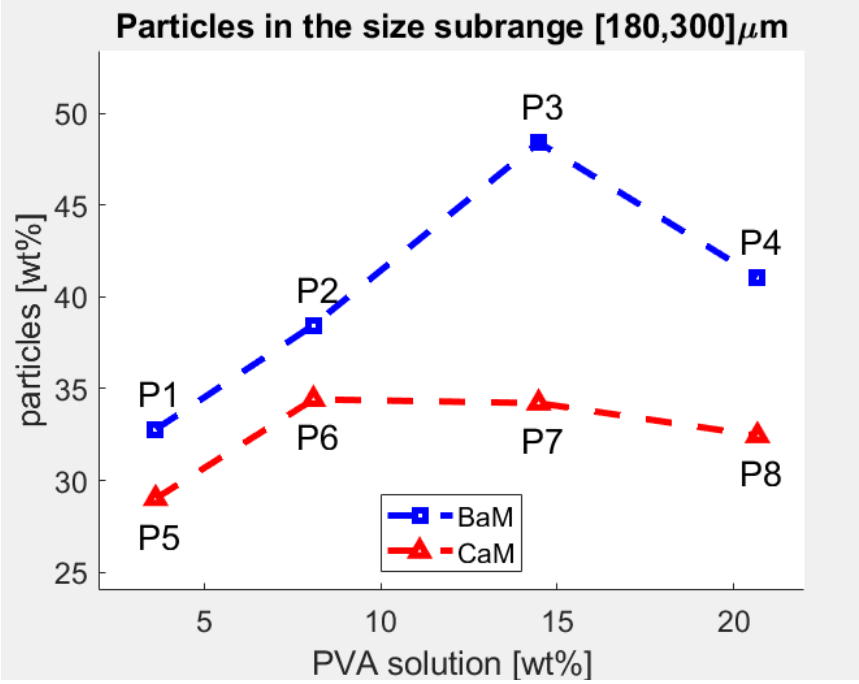

Figure 9: wt% of sample in the size subrange [180,300]µm. Plotted for samples $P1,\ldots,P8$ with respect to the amount of PVA solution added.

The test data described above together with chosen weights resulted in the decision matrix displayed in table 3. The one with the highest result was sample P3 using the BaM granulation procedure with 14.5 wt% PVA solution. A discussion taking the decision matrix and the boundaries into account, resulted in best manufacturing process for producing $CaMnO_{3-\delta}$ and the best manufacturing process for this projects continued research. The best manufacturing process according to the decision matrix is the one that produced sample P3, however BaM procedure was excluded due to it needing more ingredients per sample. Ball milling and sifting ingredients, in figure 2, took a week for producing samples $P1,\ldots,P4$ and therefore BaM procedure was excluded due to the time boundary. A manufacturing process using the CaM procedure with the highest result in the decision matrix in tabel 3 was decided to be the best for this project. Therefore the best manufacturing process for this project is the one that made P6.

Table 3: Decision matrix for samples $P1, \ldots, P8$

Criteria:	Mean crushing strength	Attrition rate	wt% in size subrange [180,300]	Cost PVA		
Weights:	0.2	-0.5	0.9	-0.1		
Process	Score				Result	Rank
P1, BaM 3.6 wt%PVA	4	3	2	1	1	6
P2, BaM 8.1 wt%PVA	7	4	5	3	3.6	2
P3, BaM 14.5 wt%PVA	3	5	10	6	6.5	1
P4, BaM 20.7 wt%PVA	1	4	6	10	2.6	4
P5, CaM 3.6 wt%PVA	2	1	1	1	0.7	7
P6, CaM 8.1 wt%PVA	9	3	3	3	2.7	3
P7, CaM 14.5 wt%PVA	10	4	3	6	2.1	5
P8, CaM 20.7 wt%PVA	7	10	2	10	-2.8	8

In summary, the P6 manufacturing process was: limestone was calcinated, manganese ore and the calcined limestone were crushed, ball milled and sieved to the size range [90,150]µm. This material was mixed, and continuously added in small batches to a plastic cup together with PVA solution while stirring with a fork. This was done until all the material was added, and the mixture contained 8.1 wt% PVA solution. The mixture was then sintered and sieved resulting in oxygen carrier particles in the size range [180,300]µm. See figure 2 and the Method section for a more detailed description.

3.2 Chemical and physical attributes

Building on the results in previous subsection, Stage 2 of the method resulted in twelve additional samples produced using the P6 manufacturing process. These samples are named $S1, S2, \ldots, S12$. This section includes results of the material strength, density, and particle structure. Chemical properties such as oxygen uncoupling and transport capacity are also included as well as the results from the techno-economic analysis.

The different sintering temperatures were decided through a temperature iteration, starting from 1215 °C. The first three samples, one of each manganese ore were sintered in a temperature of 1355 °C. It resulted in three samples: S1, S2 and S3 which all melted and fused to a solid that stuck to the crucible. The next step was then to test a lower temperature to see if the same behavior would occur. One sample, S4, was sintered in 1315°C and ended up agglomerating and fusing together to the point that the cake was unbreakable by reasonable means. To avoid the same problem

again, the temperature was lowered back to 1215°C for the remaining ores, Eramet and Braunite. The resulting samples, S5 and S6 in figure 8 was easily separated particles suitable for further testing. The last iterations were 1265 °C followed by 1240 °C, creating samples named $S7, \ldots, S12$. All these samples created suitable particles, but was increasingly harder to break apart into particles as the temperature increased. Especially hard to break apart was the samples made from the manganese ore braunite. This as the cake shrunk to the bottom of the crucible and clung to it, see S6 sample in figure 8. This made it somewhat difficult to remove from the crucible.

Table 4 below contains the stable attrition rate values attained from the jet cup attrition rig tests using equations (2) and (3). The attrition rate is closely related to the lifetime of the oxygen carrier, which is consequently one of the major factors in the operational cost of the CLC. Out of all of the samples; S8, S9, and S10 was selected for the reactivity study. Selection was based on how low their attrition rate was. The S8 sample performed the best while the S9 and S10 samples had marginally worse rates, S10 being the worst. Note that the conditions in the jet cup attrition testing rig are not very comparable to the conditions in CLC, but the values attained still provide means of comparing the produced samples.

Table 4: Attrition rate, lifetime, and mean crushing strength for the S and P samples

Sample	Attrition rate [%/h]	Corresponding lifetime [h]	Mean crushing strength [N]	Sample	Attrition rate [%/h]	Corresponding lifetime [h]	Mean crushing strength [N]
P1	4.02	24.9	0.737	S5	5.22	19.2	1.032
P2	4.28	23.4	0.864	S6	2.62	38.2	1.215
P3	4.84	20.66	0.679	S7	2.36	42.4	1.069
P4	4.30	23.3	0.592	S8	1.35	74.1	1.167
P5	2.48	40.3	0.643	S9	1.60	62.5	1.229
P6	3.76	26.6	0.922	S10	1.78	56.2	1.287
P7	4.22	23.7	0.943	S11	1.98	50.5	1.176
P8	7.69	13.0	0.839	S12	2.80	35.7	1.121
P13	3.13	31.9	1.146				

Table 5 below shows the bulk density of the samples that were chosen for further reactivity testing.

Table 5: The bulk density measured for samples S8, S9 and S10

Sample	Bulk density[g/cm^3]
S8	1.26
S9	1.21
S10	1.13

3.2.1 Oxygen carrier analysis before reactivity tests

Composition and structure analysis of the oxygen carriers were done using SEM and XRD. Oxygen carrier particles from the S9 sample, can be observed below in figure 10. S9 was produced using the manganese ore Sibelco Braunite.

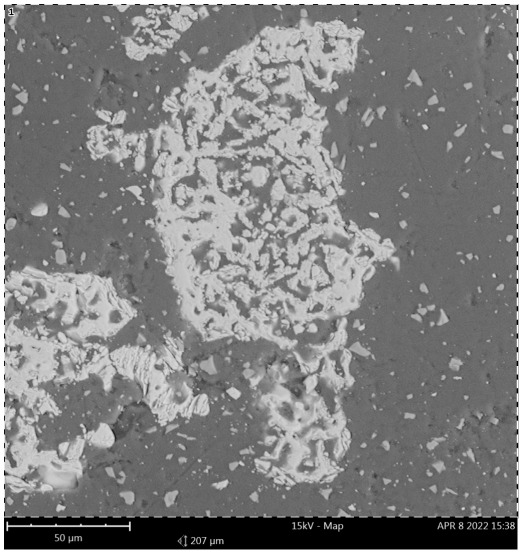

Element Number	Element Symbol	Element Name	Atomic Conc.	Weight Conc.
8	O	Oxygen	71.70	48.35
20	Ca K	Calcium	10.57	17.85
25	Mn	Manganese	10.28	23.80
14	Si	Silicon	6.02	7.13
26	Fe	Iron	1.02	2.39
13	Al	Aluminium	0.42	0.47
22	Ti	Titanium	0.00	0.00

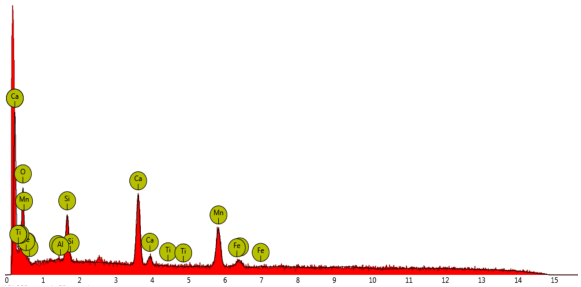

Figure 10: Fresh sample of oxygen carrier when using Sibelco Braunite as manganese ore, zoomed in at 207 µm, as well as a table showing its corresponding elemental composition and an EDX graph.

In figure 10, an image of a fresh sample of oxygen carrier and its elemental composition can be observed. The particle being showed is porous and the elemental composition shows a close to stoichiometric ratio of calcium and manganese with other impurities from the Sibelco Braunite ore also being present to a lesser extent

such a silicon, iron, and aluminium.

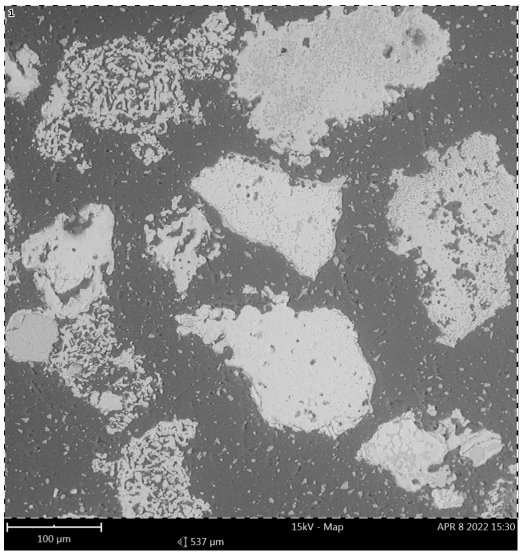

Element Number	Element Symbol	Element Name	Atomic Conc.	Weight Conc.
8	O	Oxygen	71.79	48.17
20	Ca K	Calcium	10.02	16.84
25	Mn	Manganese	9.05	20.84
14	Si	Silicon	5.52	6.50
26	Fe	Iron	2.85	6.68
13	Al	Aluminium	0.69	0.78
22	Ti	Titanium	0.10	0.20

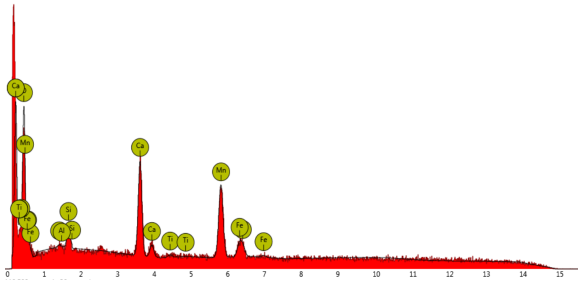

Figure 11: Several oxygen carrier particles made from Sibelco Braunite, zoomed in at 537 µm, and its elemental composition and EDX graph.

A higher variety of particles in the sample are shown in figure 11 above. This image shows that the particles vary in their porosity, from particles with a high degree to those with a low degree. The elemental composition also shows similarities to that of figure 10 but with a slightly higher concentration of impurities.

Figure 12 shows the graph for intensity against the diffraction angle for sample S9. The top four compound matches sorted by FOM are plotted as bars under the graph. The matches are filtered using the elements in figure 11.

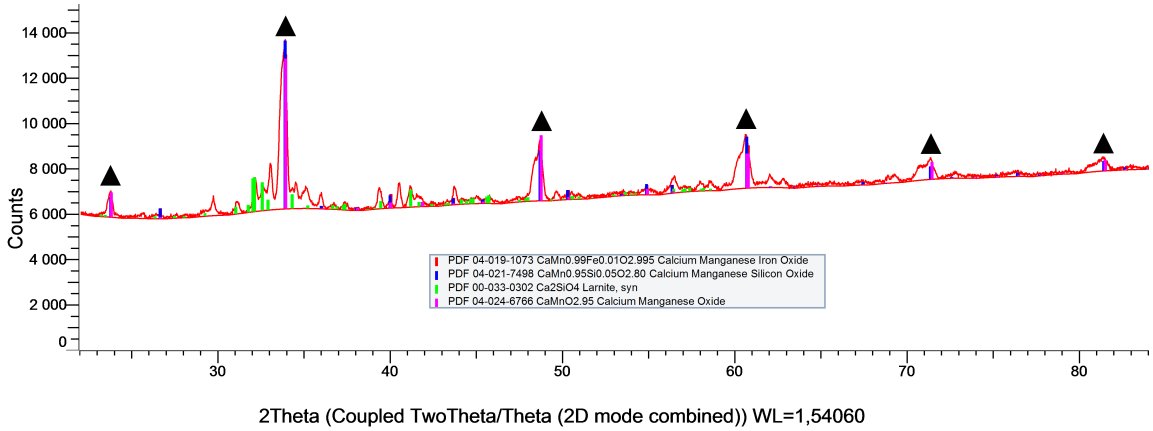

Figure 12: Graph showing intensity against the diffraction angle for sample S9. For matched compositions are shown with bars under the graph. Major peaks corresponding with a $CaMnO_{3-\delta}$ compound is marked with triangles.

Some additional matches for S9 are shown in table 6. The general result for samples P6, P13, S8, S9, and S10 is that all have the characteristic peaks marked with triangles as in figure 12. These peaks match well with previous XRD results of $CaMnO_{3-\delta}$ [23]. The top FOM compounds matched by the software are mainly $CaMnO_{3-\delta}$ or a doped version containing silicon, iron, or titanium. Doping with aluminium was not part of the top four matches for any of the samples.

Table 6: Top six compound matches for sample S9. Matched using using DIFFRAC.EVA and ranked by FOM. Before and after reaction with CH_4 in batch reactor

S9		S9 after reaction with CH_4	
FOM	Compound	FOM	Compound
41.2	$CaMn_{0.99}Fe_{0.01}O_{2.995}$	33.6	Ca_2SiO_4
39.6	$CaMn_{0.95}Si_{0.05}O_{2.8}$	23.9	$CaTi_{0.1}Mn_{0.9}O_{2.962}$
32.3	Ca_2SiO_4	23.4	$Ca_2Mn_2O_5$
31.4	$CaMnO_{2.95}$	23	$Ca_2Mn_2O_5$
29.1	$Ca_2Mn_2O_5$	22.1	$CaTi_2FeO_6$
29.0	$CaMnO_{2.8}$	21.3	$CaMn_{0.7}Fe_{0.3}O_{2.845}$

3.2.2 Oxygen uncoupling

In order to compare the oxygen uncoupling performance between the samples tested in the batch reactor, a value of oxygen uncoupling ability was calculated using equation (7) and is presented in table 7 below.

Table 7: Oxygen uncoupling ability in wt%

Sample	Pre reaction	Post reaction
S8 Methane	0.2279	0.2247
S8 Syngas used	0.2247	0.1599
S8 Syngas fresh	0.2279	0.1604
S9 Methane	0.1802	0.1770
S9 Syngas used	0.1770	0.1125
S9 Syngas fresh	0.1802	0.1197
S10 Methane	0.2347	0.2103
S10 Syngas used	0.2103	0.2192
S10 Syngas fresh	0.2347	0.2128

Table 7 shows the mean oxygen uncoupling ability obtained from oxygen release measurements. The S8 and S10 samples gave similar values around 0.21wt% in the methane test, while the S9 sample performed worst in all measurements. The uncoupling ability decreased for the S8 sample after reaction with syngas, while the S10 sample remained unaffected. In order to further analyse the oxygen uncoupling behavior, the oxygen carrier conversion was plotted during these measurements and presented in figures 13, 14 and 15.

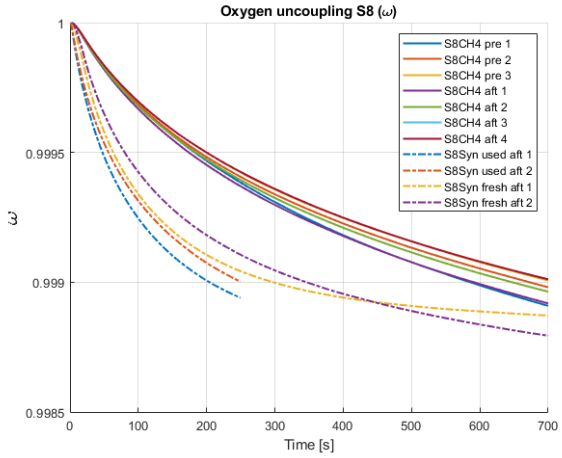

Figure 13: Plot of the oxygen carrier conversion (ω) over time during the uncoupling phase for sample S8.

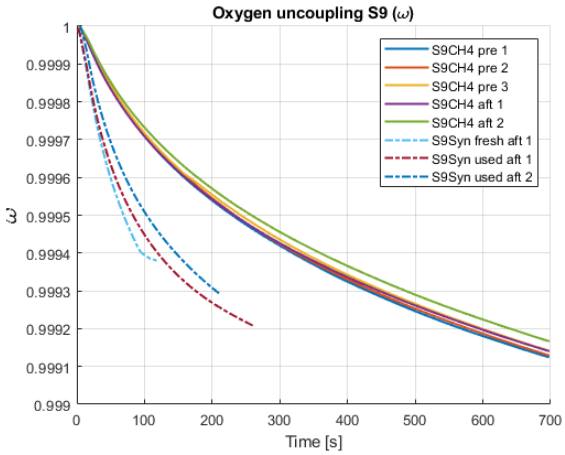

Figure 14: Plot of the oxygen carrier conversion (ω) over time during the uncoupling phase for sample S9.

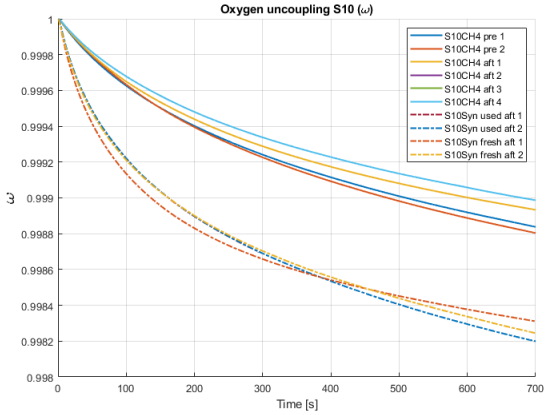

Figure 15: Plot of the oxygen carrier conversion (ω) over time during the uncoupling phase for sample S10.

Figures 13, 14 and 15 illustrate the oxygen release behavior for samples S8, S9 and S10 respectively. In all three samples the rate of oxygen release after reaction with syngas is higher than the rate before and after the reaction with methane. As can be seen from the methane lines marked 'pre' and 'aft' in each figure, the amount of

oxygen release remains largely unaffected by the reaction with methane.

3.2.3 Reactivity

Figure 16 below shows how the oxygen carrier conversion (ω) over time during the reactions. All three best performing materials (those with lowest final ω value) were all samples that had been previously reacted with methane, indicating activation of the oxygen carrier. Figure 17 shows the derivative of the the previously mentioned oxygen carrier conversion results, that is the rate of oxygen release during the tests. Figures 18 and 19 show an examples of how the ω value changes during the reaction for the S8 sample reaction with methane and syngas. The change in ω over time is proportional to the amount of oxygen leaving the reaction chamber, calculated by equation (12).

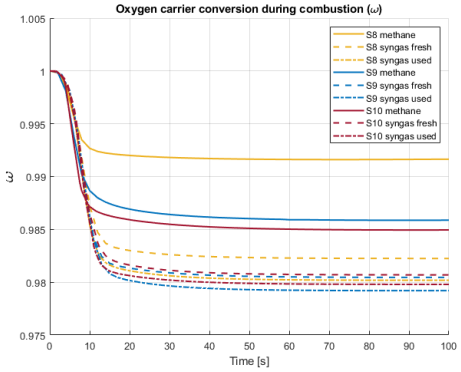

Figure 16: Plot of the oxygen carrier conversion (ω) over time during the reactions with methane and syngas.

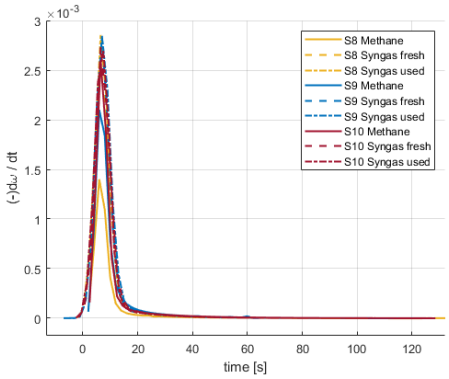

Figure 17: Plot of the oxygen carrier conversion derivative ($\dot{\omega}$) over time during the reactions with methane and syngas.

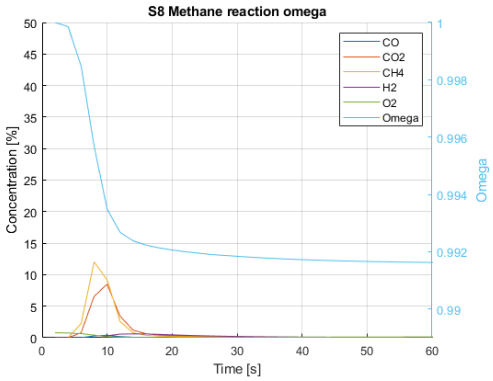

Figure 18: example illustrating how the ω value varies during the reaction of the S8 sample with methane gas.

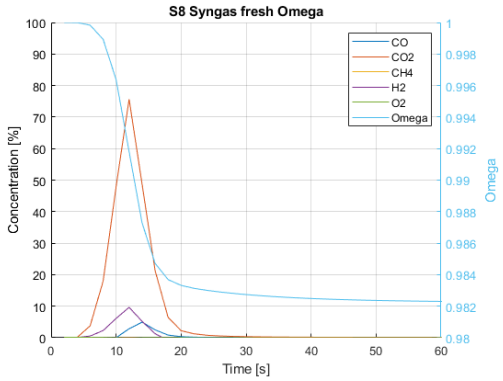

Figure 19: example illustrating how the ω value varies during the reaction of the S8 sample with syngas.

Table 8 shows the oxygen transport capacity values calculated by equation (12) . As was seen in figure 16 the best performing material was the methane reacted S9 sample during reaction with syngas.

Table 8: Oxygen transport capacity calculated during combustion of the samples with methane and syngas

Sample	Oxygen transport capacity[2] (wt%)
S8 Methane	0.83
S8 Syngas used	1.98
S8 Syngas fresh	1.78
S9 Methane	1.41
S9 Syngas used	2.08
S9 Syngas fresh	1.99
S10 Methane	1.5
S10 Syngas used	2.019
S10 Syngas fresh	1.93

3.3 Fuel conversion

Figure 20 below shows the fuel conversion γ plotted against the oxygen carrier conversion ω during the reaction with syngas. All of the samples maintain a high fuel

conversion throughout the reaction, with a slight continuous decrease with falling oxygen content in the carrier.

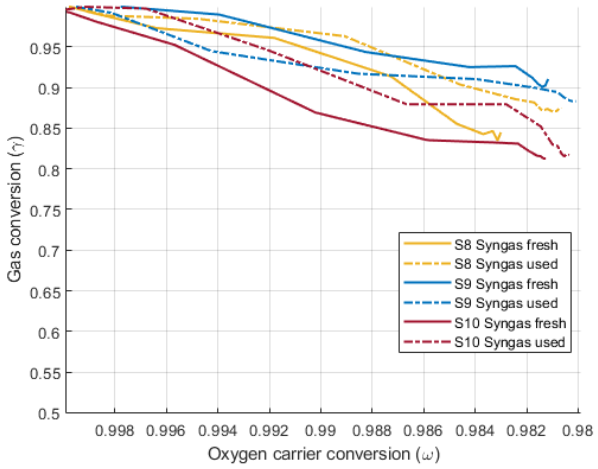

Figure 20: Plot of the gas conversion (γ) against the oxygen carrier conversion (ω) during the reactions with syngas.

3.3.1 Oxygen carrier analysis after reactivity tests

In figure 21 and 22 below, the effects after being reacted with methane during the reactivity tests performed can be observed.

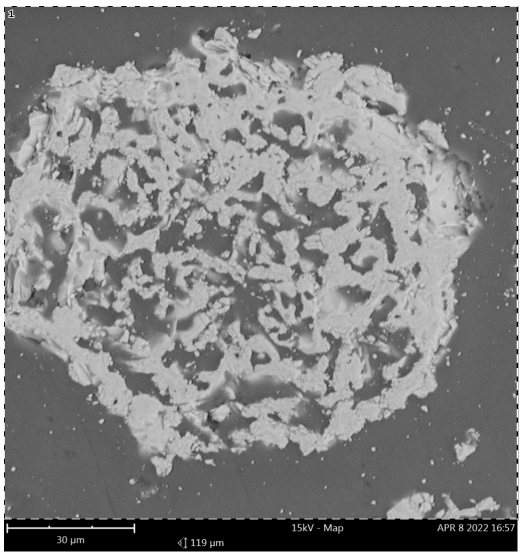

Element Number	Element Symbol	Element Name	Atomic Conc.	Weight Conc.
8	O	Oxygen	72.57	47.86
20	Ca K	Calcium	14.21	23.48
25	Mn	Manganese	10.78	24.41
26	Fe	Iron	1.28	2.95
13	Al	Aluminium	0.61	0.68
14	Si	Silicon	0.54	0.63
22	Ti	Titanium	0.00	0.00

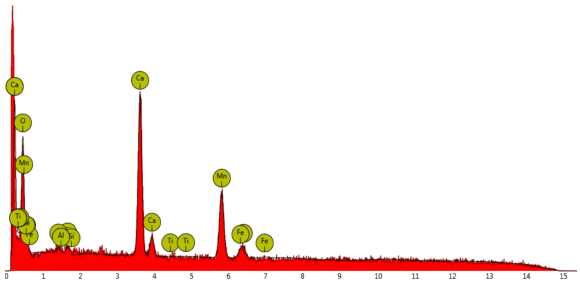

Figure 21: Single oxygen carrier particle made from Sibelco Braunite after being subjected to methane zoomed in at 119 µm, a table of its elemental composition and an EDX graph.

The particle observed in figure 21 shows a high porosity, similar to that observed before reactivity test in figure 10. The elemental composition presented in figure 21 also shows a difference in atomic concentration between calcium and manganese suggesting not all particles have a stoichiometric ratio. Low amounts of impurities are also present.

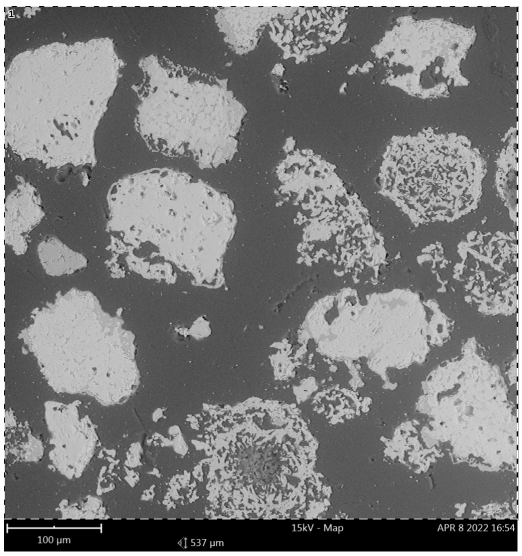

Element Number	Element Symbol	Element Name	Atomic Conc.	Weight Conc.
8	O	Oxygen	74.33	49.25
25	Mn	Manganese	12.08	27.49
20	Ca K	Calcium	8.69	14.43
26	Fe	Iron	2.54	5.87
14	Si	Silicon	1.78	2.07
13	Al	Aluminium	0.30	0.33
22	Ti	Titanium	0.28	0.56

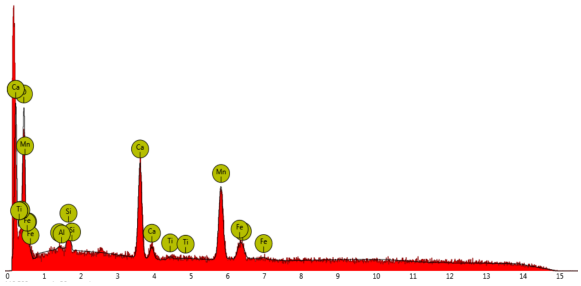

Figure 22: A picture showing several particles subjected to methane, zoomed in att 537µm, and its elemental composition together with its EDX graph.

When several particles are studied as shown in figure 22 the high variation of porosity remains as also seen before reactivity tests in figure 11. The element composition also shows the difference in atomic concentration between calcium and manganese, similar to 21, and a higher amount of impurities in the sample.

3.4 Techno-economic analysis

Based on the attrition results, presented in table 4 from Stage 1, and oxygen transport capacity, presented in table 8 from Stage 2, an estimate of the amount of material required for a 1MW CLC system can be calculated. Following this, the cost of production is done by proposing industrial scale machinery and calculating the annual electricity cost based on the components motor power, using bulk density 5 and assuming 8000 hours of operation time per year. The $\frac{d\omega}{dt}$ that is used for material costs is an average between ω being 1 och 0.99 which can be seen in figures 16 and using the value from figure 17 which in this case results in $\frac{d\omega}{dt} = 1.5 * 10^{-3}[\frac{1}{s}]$.

3.4.1 Material cost

A techno-economic analysis was done to evaluate how feasible scaling up would be with respect to the cost and the method. The techno economic analysis was done with the same syngas samples which were used in the reactivity tests as methane results seemed unreliable. The attrition rates used in this analysis are shown in table 4 and their reactivity in table 8.

Table 9: Material and costs required for reactors with syngas as fuel initially and yearly

Sample	Concurrent mass air reactor [kg]	Concurrent mass fuel reactor [kg]	Initial total cost [SEK]	Yearly fresh flow [kg/year]	Yearly cost [SEK/year]
S8 Syngas fresh/used	41	41	1176	8786	126292
S9 Syngas fresh/used				10414	149680
S10 Syngas fresh/used				11586	166520

The concurrent mass required for the air reactor and fuel reactor in order to provide enough oxygen to support the combustion reaction and the yearly fresh flow of oxygen carrier needed due to the attrition, is displayed in table 9. The table also displays the initial cost which is the cost of the first batch, as well as the cost of the yearly flow. From table 9 it can be seen that a minimum of 41 kg oxygen carrier is needed in the fuel reactor at all times to provide enough oxygen for the fuel combustion. The mass is the same for all the samples since the value for $\frac{d\omega}{dt}$ is the same. The main expense is the yearly cost due to attrition, since the initial mass needs to be completely replaced approximately 100-140 times each year depending on the sample. The table also shows that a difference in attrition rate of 0.043 %/h between S8 and S10 result in the cost varying approximately 3f0000 SEK/year (S8 syngas fresh/used and S10 syngas fresh/used).

3.4.2 Manufacturing cost

Table 10: The yearly cost of calcination and sintering for each sample

Sample	Initial cost of calcination [SEK]	Yearly cost of calcination [SEK/year]	Initial cost of sintering [SEK]	Yearly cost of sintering [SEK/year]
S8 Syngas fresh/used	1614	174240	6522	704436
S9 Syngas fresh/used		206506		834886
S10 Syngas fresh/used		229728		928810

Table 10 displays the initial costs of calcining the required limestone to produce the calcium needed for the first batch of $CaMnO_{3-\delta}$. The table also shows the initial cost of sintering said amount of $CaMnO_{3-\delta}$ which is shown in table 9. Along with the initial costs table 10 also show the cost of calcining and sintering the materials needed every year. From table 10 it is visible that the cost of sintering, both the initial and yearly, is higher than the cost of calcination but still within the same order of magnitude.

For the remaining machinery the estimated electricity cost per year is 68 SEK for mixing, 672 SEK for ball milling and 46 SEK for sieving. The estimated costs is based on a mean of the yearly mass flow values calculated in table 9.

4 Discussion

This section discusses the result of the project. The result is viewed from several perspectives. Mainly, what conclusions can be drawn from the results, and what possible subjects are there for future research.

4.1 Method

As seen in figure 9 the BaM method produced more particles within the subrange of [180,300]µm. This leads to a belief that BaM could be more effective for a CLC system as more particles in this size range leads to better combustion performance. The CaM method lacks this favorable result which leads to the assumption that the particle performance for CaM would not be as good. Another difference between the two methods, BaM and CaM, is the needed equipment and therefore the time needed to prepare sufficient material. The food processor used in the BaM method requires more material to blend the mixture homogeneously, compared to the CaM method which uses a smaller container to mix the material. This is the underlying reason for using CaM in Stage 2 and 3 even though the results in Stage 1 (See table 3) show that BaM, specifically the method used to produce the P3 sample, might be the better method. However, it is also possible that the manufacturing process for making P13 is better but this is uncertain due to lack of data. The original idea was that if the limestone was not calcined it would negatively affect the integrity of the particle since CO_2 would instead be released in the sintering process instead of during the calcination. This speculation was however weakened by the crushing strength test and attrition test on the P13 particles, where the results were not substantially worse, in fact it was amongst the best. This was discovered at a later stage in the research and since a sizable amount of limestone already had been calcined and ball milled the research was continued with the calcined limestone. During the mixing of materials, specifically when PVA solution was added, it was observed that the mixture would rapidly increase in temperature due to the calcium oxide reacting with the water in the PVA solution. A better understanding of the phenomena and the effects of the heat release could lead to improvements in future research. One possible avenue of research is heating the limestone even higher during the calcination, as this forms so called "dead burned" lime which reacts far slower with water[37], possibly negating any effects of the heat generated.

After sifting the crushed ores, not all of the sizes were used for further production of the oxygen carriers. Particles above the size of 300 µm were deemed too

large for production requirements and those lower than 90 μm were considered very time-consuming to prepare as well as possibly producing too small oxygen carriers. In hindsight, it could have been a good idea to use the smaller sized ores as well, as those combined have a larger total surface area on which the reaction between manganese and limestone could occur. Using smaller sized material could also contribute to a more homogeneous material as the distribution and mix would be better. In addition, the used production method was based on adding more material over time. The smaller sizes of material in combination with the binder could possibly have made them stick on the outside of the larger previously formed particles to make them bigger and more homogenized. Therefore, it could be a good idea to first form bigger particles and then later sprinkle smaller sized material on top them. Another option would be to use the smaller material already from the beginning which may make the particles more dense.

Other production methods could also be tried to see if they give better results in for example how the fines combine. An example of another production method could be an extruder combined with a spheronizer [21]. This method could contribute to avoid having such a wide size distribution of the manufactured material and therefore have more produced material come to use in a CLC. A cost estimation for the extruder-spheronizer has not been done, so researching and comparing it to the production method described in this report could be interesting. Furthermore, the ores that were chosen for this project were as mentioned selected because of their high concentration of manganese, accessibility both in the lab but also in the global market. Since the ores are not pure and contains other substances which change their characteristics, an interesting point could be to use other manganese and limestone ores and see if the results would change and if so, how? Furthermore, other parameters such as stoichiometric compositions could be investigated as it in this project did not vary from a 1:1 ratio. Either by using more manganese or more limestone when mixing, some reactions might be favored while others are not.

4.2 Physical attributes

As seen in the results for crushing strength and attrition, the produced materials are not durable. The lowest accepted result from the crushing strength test was 1 N. While the particles did have better results (See table 4) it was still relatively low which indicates that the particles will easily crush upon impact in a reactor. The oxygen carriers will travel back and forth as well as be a part of the fluidized bed

which makes good results for attrition and crushing strength all the more important. Table 4 shows a very short lifetime which is connected to the sintering temperature used. Sintering at a relatively high temperature resulted in the samples melting or agglomerating, forcing the other samples to be sintered at lower temperatures making them less durable. A possible explanation for this is that the cheap ores had many impurities which affected the material characteristics. Since attrition rate is directly dependent on the sintering process, researching the sintering process could prove beneficial in order to get a better attrition rate and thereby solving the biggest problem with the particles produced with this method. A good starting point could be to explore other sintering temperatures and preferably go higher. Linked to this, one could also investigate how the duration at the highest temperature in the oven effects the hardness of the oxygen carriers [21] since the sintering process was done over twelve hours in total, nine of which was at the sintering temperature specified for each sample. It is notable to mention that the crushing strength test was performed manually and therefore leave a lot of room for errors. While crushing strength is very important, the test results are unreliable and are therefore not of the highest importance.

4.3 SEM and XRD

As seen in figure 10, 11, 21 and 22 the SEM pictures show that the difference between the particles that were fresh and particles that had been subjected to methane gas showed similar structures. This shows that the structural integrity seemed to be stable due to not being able to observe cracks in the particles. It can also be seen that the particles elemental composition showed similarities but also differences. For the fresh material the concentration between calcium and manganese seemed closer than after tests with methane were done. Impurities also seemed to become lower after tests were performed. To develop this for the future, more cycles in the batch reactor could be run to better see how the particles break down over time and perhaps see bigger changes in the structure using the SEM.

As the placement of the major peaks in figure 12, and the rest of the samples, matched very well with previous research on $CaMnO_3$ [23]. It can be concluded that the manufacturing processes produced the desired calcium manganate material, and that it works with different ores and temperatures.

4.4 Reactivity and oxygen uncoupling

When inspecting figures 13, 14 and 15 it is easy to see the impact the reaction with syngas has. The reaction with syngas results in faster oxygen release, however the amount released does not increase as can be seen in table 7. In fact, the reaction with syngas generally decreased the oxygen uncoupling ability for the samples tested. Although the oxygen uncoupling ability decreased after reaction, the reverse was seen in the total oxygen transport capacity. Table 8 and figure 16 show that for all samples the reaction with methane increased the total oxygen transport capacity for subsequent reaction with syngas. A hypothesis for the increased oxygen transport capacity after reaction with methane gas is etching of the surface, which could lead to a larger surface area and better transport performance. It is also notable to mention that for all samples the total amount of oxygen given off for combustion reactions is larger when using syngas as fuel compared to methane, this can be attributed to the higher reactivity of syngas which causes further reduction of the oxygen carrier. All samples reacted with syngas show very similar performance by the close grouping in figure 16 as well as the nearly identical derivatives in figure 17. The gas conversion results presented in figure 20 were also generally good in all samples reacted with syngas. All samples maintained a gas conversion above 80% throughout the depletion cycle, with sample S9 maintaining above 90%.

Comparing the oxygen transport capacity and the oxygen uncoupling ability presented in the previously mentioned tables shows that the materials all have a poor ratio of oxygen able to be released as gas, compared to the amount that can be given off for combustion reactions. The materials are generally only able to release 0.2wt% O_2 as gas, while they are able to transport 2wt% for fuel reaction. The poor oxygen release ability can be partially attributed to the integration method used, calculating the amount released from 1 vol% O_2 to 0.1 vol% O_2 output flow concentration. This was done due to time constraints, as measuring until the concentration reached zero would have likely required twice as long injection of nitrogen and thus been unfeasible due to the time constraints.

It is important to mention that the batch reactor test was plagued by a number of issues relating to the equipment, the most significant of which was that the total molar amount of carbon leaving the reactor after injection of methane was only 10% of the injected amount. The cause of this is still unknown, however due to the carbon balance for syngas reactions being ideal, we assumed that the proportionality of the detected CO and CO_2 in the methane reactions was correct and simply calculated a new theoretical flow rate which would have given perfect carbon balance. As

such, any values obtained through the methane reactions should not be compared to other literature, however this only applies to reaction specific data (estimated oxygen transport capacity) and not oxygen uncoupling. A possible explanation for the issue was the long refresh rate of the gas analyzer, due to the reaction happening very fast it may well have failed to detect a large portion of the combustion products. Notably the equipment issues lead to unreasonable results when plotting the gas conversion against oxygen carrier conversion, a large rise in fuel conversion with depleting oxygen content in the carrier. As these results are unrealistic and the methane reaction tests already known to have been affected by equipment issues, we chose not to include these in the work.

4.5 Upscaling

The concurrent masses required for each sample displayed in table 9 show that all the samples have the same results initially. The pattern of the yearly fresh flow of oxygen carrier differs from the pattern mentioned above and instead follows the attrition results shown in table 4. The samples with the best result with regards to the yearly flow is S8 syngas fresh/used as it had the best attrition rate of the 3 samples. Both the initial and the yearly cost is linearly dependent on these masses and therefore follow the same pattern as their respective mass. The initial costs of calcination and sintering seen in 10 are also linearly dependent on the respective masses and therefore follow the same pattern as those for the material costs and shows that S8 syngas fresh/used was the cheapest.

When researching which starting method should be used, one of the requirements was that it could be used in a larger scale. The BaM method, which used a food processor, was the starting point as the bowl in the processor could be seen as a industrial mixer and would in theory be easy to scale up. Cost of heating is the majority of the expenses, as can be seen in table 10, and leave much room for improvements as it is approximately 87 % of the total yearly cost. Table 10 also show that the cost of sintering is noticeably higher than the cost of calcining due to the high temperature sintering oven having a higher cost per hour as well as a smaller capacity meaning more batches are required. The cost of mixing, sieving and ball milling can be considered more or less negligible when compared to the material costs and the heating costs. Scaling these three up to an industrial scale is very well feasible as the cost is relatively low and the required machinery already exists and is used in other industries. Cost of materials on the other hand are high due to the concurrent mass needing to be completely replaced approximately 200 times every

year due to attrition and therefore presents an issue when scaling up. However, the main problem found through the techno-economic analysis is still the cost of heating.

A vast majority of the manufacturing expenses are due to the ovens used for calcining and sintering as can be seen in table 10. The cost of sintering is noticeably higher than calcining due to the high temperature sintering oven having a higher cost per hour as well as a smaller capacity meaning more batches are required. Decreasing the duration in the oven could prove to be vital in improving the results of this project since this could heavily decrease the overall cost.

A solution to both of these problems would be to decrease the yearly flow of oxygen carriers by improving either the lifetime of the particle or their oxygen transport capabilities. As both of these attributes are heavily affected by the temperature used in the sintering process, a priority in order for further development should be improving the sintering process. By researching the sintering process, the particles could be sintered at a high temperature so that they have a better attrtion rate without melting, agglomorating to an extreme amount nor loose their reactivity. This research could also help to decrease the duration in the oven which could prove to be vital in decreasing the cost of sintering and improving the results of this project since this could heavily decrease the overall cost. Testing the particles in an actual chemical-looping combustion process will also give more insight into the actual lifetime the particles can achieve which could be much more than the values used for calculations in this work.

5 Conclusion

While the BaM method showed better yield of $CaMnO_{3-\delta}$ particles in the desired size range of [180,300]µm, due to the time constraints further investigation of the method was not viable for this report. Using the CaM method an observation was made that the optimal amount of 10wt% PVA binder solution was 8.1wt% in the manganese ore and CaO mixture, sintering at 1265°C resulted in the lowest attrition rate. However, the attained attrition rate results are still significantly higher than what is viable for commercial CLC. The best lifetime of the samples tested was only 74.1h but this should be further tested in more realistic environments.

Out of the samples tested in the batch reactor, the S9 sample produced from Sibelco Braunite had the best performance. After activation of the particles with methane, the oxygen transport capacity measured by reaction with syngas was 2.08wt%. Reaction with syngas increased the rate of oxygen uncoupling, but lowered the total amount able to be uncoupled from 0.177wt% to 0.11wt%. CLOU properties were detected in all tested samples, however they were consistently unimpressive.

The techno-economic analysis approximated the yearly cost of raw materials at 127906 $SEK/year$ and the operating costs at 879462 $SEK/year$ for S8 syngas fresh/used, which was the sample with the best result with regard to costs. Along with the cost, the analysis showed a required concurrent mass in the fuel and air reactor of 41 kg and a yearly fresh flow of 8786 kg for a 1MW reactor. The yearly flow, which is required due to the attrition, shows that the concurrent mass would need to be completely replaced approximately 200 times every year. The main expense for production was heating, as it is responsible for 87 % of the yearly operating cost.

Throughout the results it is evident that further research is required before considering commercial use. The main focus should be to investigate the lifetime of the particles, which during techno-economic calculations was a low estimation; replacing the concurrent mass 200 times every year is not economically viable. We suggest further research into lowering the attrition rate as that is currently the biggest issue with the produced $CaMnO_{3-\delta}$ materials. The sintering process used in this project has not been researched thoroughly and have potential for improvement, for example the duration and the highest temperature are factors that may have large impact on physical and reactive performance. Other suggestions proposed in this project is to research the effect of $Ca(OH)_2$ forming during the mixing step, as the heat release is substantial and may well have an impact on produced material.

References

[1] Tidskriften havsutsikt. Hur påverkas djuren i havet av försurning? https://www.havet.nu/havsutsikt/artikel/hur-paverkas-djuren-i-havet-av-forsurning. Accessed: 19.04.2022.

[2] Sveriges miljömål. Begränsad klimatpåverkan. https://www.sverigesmiljomal.se/miljomalen/begransad-klimatpaverkan/. Accessed: 19.04.2022.

[3] World Health Organization. Climate change and human health. https://www.who.int/news-room/fact-sheets/detail/climate-change-and-health, Oct 2021. Accessed 12.05.2022.

[4] J.Marsch. How does climate change affect plants and animals? https://environment.co/how-does-climate-change-affect-plants-and-animals/.

[5] Anders Lyngfelt, Bo Leckner, and Tobias Mattisson. A fluidized-bed combustion process with inherent co2 separation; application of chemical-looping combustion. *Chemical Engineering Science*, 56(10):3101–3113, 2001.

[6] European Commission. Why do we need carbon capture, use and storage? https://ec.europa.eu/clima/eu-action/carbon-capture-use-and-storage_en. Accessed: 19.04.2022.

[7] Juan Adanez, Alberto Abad, Francisco Garcia-Labiano, Pilar Gayan, and Luis F. De Diego. Progress in chemical-looping combustion and reforming technologies. *Progress in Energy and Combustion Science*, 38(2):215–282, 2012.

[8] Tobias Mattisson, Anders Lyngfelt, and Henrik Leion. Chemical-looping with oxygen uncoupling for combustion of solid fuels. *International Journal of Greenhouse Gas Control*, 3(1):11–19, 2009.

[9] Anders Lyngfelt. Chemical looping combustion: Status and development challenges. *Energy & Fuels*, 34(8):9077–9093, 2020.

[10] Tobias Mattisson, Martin Keller, Carl Linderholm, Patrick Moldenhauer, Magnus Rydén, Henrik Leion, and Anders Lyngfelt. Chemical-looping technologies using circulating fluidized bed systems: Status of development. *Fuel Processing Technology*, 172:1–12, 2018.

[11] Magnus Rydén, Anders Lyngfelt, and Tobias Mattisson. Camn0.875ti0.125o3 as oxygen carrier for chemical-looping combustion with oxygen uncoupling (clou)—experiments in a continuously operating fluidized-bed reactor system. *International Journal of Greenhouse Gas Control*, 5(2):356–366, 2011.

[12] Magnus Rydén, Anders Lyngfelt, and Tobias Mattisson. Camn0.875ti0.125o3 as oxygen carrier for chemical-looping combustion with oxygen uncoupling (clou)—experiments in a continuously operating fluidized-bed reactor system. *International Journal of Greenhouse Gas Control*, 5(2):356–366, 2011.

[13] Patrik Moldenhauer; Magnus Rydén; Tobias Mattison; Anders Lyngfelt. Chemical-looping combustion and chemical-looping with oxygen uncoupling of kerosene with mn- and cu-based oxygen carriers in a circulating fluidized-bed 300 w laboratory reactor. `https://publications.lib.chalmers.se/records/fulltext/local_164302.pdf`. Accessed: 22.03.2022.

[14] Mahdi Yazdanpanah, Ann Forret, and Thierry Gauthier. Impact of size and temperature on the hydrodynamics of chemical looping combustion. *Applied Energy*, 157:416–421, 2015.

[15] Matthias Schmitz and Carl Johan Linderholm. Performance of calcium manganate as oxygen carrier in chemical looping combustion of biochar in a 10kw pilot. *Applied Energy*, 169:729–737, 2016.

[16] Abdul-Majeed Azad, Ali Hedayati, Magnus Rydén, Henrik Leion, and Tobias Mattisson. Examining the cu-mn-o spinel system as an oxygen carrier in chemical looping combustion. *Energy Technology*, 1(1):59–69, 2013.

[17] Patrick Moldenhauer, Peter Hallberg, Max Biermann, Frans Snijkers, Knuth Albertsen, Tobias Mattisson, and Anders Lyngfelt. Oxygen-carrier development of calcium manganite–based materials with perovskite structure for chemical-looping combustion of methane. *Energy Technology*, 8(6):2000069,

2020.

[18] Peter Hallberg, Magnus Rydén, Tobias Mattisson, and Anders Lyngfelt. Camno3- made from low cost material examined as oxygen carrier in chemical-looping combustion. *Energy Procedia*, 63:80–86, 2014. 12th International Conference on Greenhouse Gas Control Technologies, GHGT-12.

[19] Octave Levenspiel. *Chemical Research Engineering*. Wiley, 1998.

[20] Marijke Jacobs, Tjalling Van Der Kolk, Knuth Albertsen, Tobias Mattisson, Anders Lyngfelt, and Frans Snijkers. Synthesis and upscaling of perovskite mn-based oxygen carrier by industrial spray drying route. *International Journal of Greenhouse Gas Control*, 70:68–75, 2018.

[21] Yunchang Dong, Yanan Wang, Jinchen Ma, Hengfeng Bu, Chuanbao Zheng, and Haibo Zhao. Binary-ore oxygen carriers prepared by extrusion–spheronization method for chemical looping combustion of coal. *Fuel Processing Technology*, 221:106921, 2021.

[22] J. Hermansson. Granulering i hushållsassistent. *Informationsblad, 'Kemira Chemicals'*, 1993.

[23] Izaskun Gil De Muro, Maite Insausti, Luis Lezama, and Teófilo Rojo. Morphological and magnetic study of camno3x oxides obtained from different routes. *Journal of Solid State Chemistry*, 178(3):928–936, 2005.

[24] Luis F.de Diego; Alberto Abad; Arturo Cabello; Pilar Gayán; Fransisco García-Labiano; Juan Adánez. Reduction and oxidation kinetics of a $camn_{0.9}mg_{0.1}o_{3-\delta}$ oxygen carrier for chemical-looping combustion. `https://doi.org/10.1021/ie4015765`. ind. Eng. Chem. Res. 2014, 53, 1, 87–103 Accessed: 19.04.2022.

[25] Daofeng Mei, Amir H. Soleimanisalim, Anders Lyngfelt, Henrik Leion, Carl Linderholm, and Tobias Mattisson. Modelling of gas conversion with an analytical reactor model for biomass chemical looping combustion (bio-clc) of solid fuels. *CHEMICAL ENGINEERING JOURNAL*, 433(2), APR 1 2022.

[26] Henrik Leion, Anders Lyngfelt, Marcus Johansson, Erik Jerndal, and Tobias

Mattisson. The use of ilmenite as an oxygen carrier in chemical-looping combustion. *Chemical Engineering Research and Design*, 86(9):1017–1026, 2008.

[27] Dazheng Jing, Frans Snijkers, Peter Hallberg, Henrik Leion, Tobias Mattisson, and Anders Lyngfelt. Effect of production parameters on the spray-dried calcium manganite oxygen carriers for chemical-looping combustion. *Energy Fuels*, 30(4):3257–3268, 2016.

[28] A. Abad, F. García-Labiano, P. Gayán, L.F. De Diego, and J. Adánez. Redox kinetics of camg0.1ti0.125mn0.775o2.9 for chemical looping combustion (clc) and chemical looping with oxygen uncoupling (clou). *Chemical Engineering Journal*, 269:67–81, 2015.

[29] Manganese statistics and information. `https://www.usgs.gov/centers/national-minerals-information-center/manganese-statistics-and-information`, 2022.

[30] How much does crushed stone and gravel cost? `https://homeguide.com/costs/gravel-prices`, 2022.

[31] 100g Polyvinyl Alcohol (PVA). Polyvinyl alcohol (pva), 100g for sale. buy from the science company. `https://www.sciencecompany.com/Polyvinyl-Alcohol-PVA-100g-P16670.aspx`, 2022.

[32] Milligan Dave, Engström Ulf, and Smith Steven. High temperature sintering – a cost effective way to future high performance materials. `https://www.hoganas.com/globalassets/download-media/technical-papers/pm/hightemperaturesinteringacosteffectivewaytofuturehighperformancematerials.pdf`, 2022.

[33] Stigande elpriser varierar kraftigt i norr och söder. `https://www.scb.se/hitta-statistik/redaktionellt/new-stigande-elpriser-varierar-kraftigt-i-norr-och-soderpage/`.

[34] Mining equipment secondary stage grinding materials advanced technology ball mill. `https://stmmachine.en.made-in-china.com/product/fdSAFGPvnrpy/`

China-Mining-Equipment-Secondary-Stage-Grinding-Materials-Advanced-Technology-Ba
html.

[35] Horizontal mixing machine putty powder/blender/detergent powder/feed/ribbon mixer. https://kdmachine.en.made-in-china.com/product/VSnmrUXcHyRM/China-Horizontal-Mixing-Machine-Putty-Powder-Blender-Detergent-Powder-Feed-Ribbo
html.

[36] Fine powder screening rotary vibrating sieve machine on sale. https://xxjubao.en.made-in-china.com/product/dFyJSkwVKHWs/China-Fine-Powder-Screening-Rotary-Vibrating-Sieve-Machine-on-Sale.
html.

[37] W. A. Cunningham. Fundamentals of lime burning. *Industrial Engineering Chemistry*, 43(3):635–638, 1951.